The Version of Record of this manuscript has been published and is available in The International Journal of Fatigue Volume 124, July 2019, Pages 236-244 https://doi.org/10.1016/j.ijfatigue.2019.03.001

Fatigue life assessment of a Short Fibre Reinforced Thermoplastic at high temperature using a Through Process Modelling in a viscoelastic framework

Nathan Fouchier[1], Carole Nadot-Martin[1*], Edoardo Conrado[2], Andrea Bernasconi[2], Sylvie Castagnet[1]

[1]Institut Pprime (UPR 3346 CNRS – ISAE-ENSMA – University of Poitiers), Department of Physics and Mechanics of Materials, Poitiers, France

[2] Politecnico di Milano, Dipartimento di Meccanica, Milano, Italie

* Corresponding author: carole.nadot@ensma.fr

Abstract: A Through Process Modelling (TPM) fatigue life assessment methodology – previously validated in an elastic framework for Short Fibre Reinforced Thermoplastics at room temperature– was extended to high temperature. The viscoelasticity of the matrix was taken into account to estimate the local effective mechanical properties at any point, from the knowledge of local fibre orientation provided by the simulation of injection-moulding. Lifetime estimation was obtained from an energetic fatigue criterion applied in the stationary regime. The approach was validated from uniaxial fatigue tests conducted at 110°C in tension, in PA66GF30 samples cut out from injected plates with three different orientations to the injection direction, at two stress ratios (0.1 and -1).

Keywords: PA66GF30; Viscoelasticity; Through Process Modelling; Homogenization; Energetic fatigue criterion.

1. Introduction

The use of composite materials as replacement of metallic alloys has been growing in

automotive and aeronautic industry. Injection-moulded Short Fibre Reinforced Thermoplastics (SFRT) and especially reinforced Polyamides have been widely used for structural parts.

The industrial design of parts requires numerical tools to assess their fatigue life under operating conditions. Different types of design methodology exist in the literature. Two main families could be distinguished. In approaches based on *non-linear constitutive laws*, the cyclic behaviour was continuously described using an evolution law of damage, for all or part of fatigue life [1-4]. This kind of approach was explicit but expensive regarding calculation and identification times. On the other hand, *fatigue-criterion* approaches directly connected a Fatigue Indicator Parameter (FIP) –calculated from the mechanical response over a stabilized cycle– to the number of cycles to failure. Damage evolution was not explicitly depicted; the challenge was to capture the key factors governing fatigue life into the FIP and the fatigue criterion equation. Such approaches were suitable when crack initiation occurred over a major part of the lifetime. Different criteria were proposed in the literature, based on equivalent stresses [5–8] or energy [5, 6, 9]. For this type of materials and at ambient temperature, the most recent works suggested to opt for energy-based criteria [5, 6].

Fatigue-criterion approaches have been widely used in industrial context, due to the possibly reduced calculation and identification time. In order to apply the fatigue criterion, the FIP should be calculated over a stabilised cycle or at least over a cycle on which it is stabilised. The cyclic behaviour and the fatigue strength of SFRT widely depended on the fibres orientation distribution (FOD) that was locally heterogeneous in an injected part [6], [8], [10]–[12], on the environment conditions, i.e. temperature ([7], [10], [13], [14]) and, in the case of hydrophilic polymers like polyamides, on the moisture content that plays a similar role ([10], [15]–[17]). The environment effect could be taken into account through the gap of temperature between the operating and glass transition ones [16]. Gathering all these

influence factors (viscoelasticity, viscoplasticity, anisotropy, multi-physical coupling) into a constitutive law is still an open issue. Thus, most of modellings employed as input calculations for fatigue-criterion approaches only retained some of them. Heterogeneity of fibre orientation and induced anisotropy should be a priority. In the literature, both phenomenological [18], [19] and micromechanical descriptions [6], [20] were used to this aim.

Because of the few experimental tests performed at higher temperature, most of the fatigue design model were proposed at room temperature. But the trend to use injected parts close to hot zones has been requiring the development of a life assessment tool suitable for higher temperatures.

This was the main objective of the present work. A Through Process Modelling (TPM) for fatigue life assessment of SFRT was developed for a polyamide-based composite (PA66GF30) at 110°C. The approach was extended from the TPM initially developed by Klimkeit et al. [6], validated for several SFRT at room temperature considering an elastic behaviour of the matrix. It was a fully integrated numerical approach linking the injection simulation to the estimate of the fatigue life. The TPM methodology was made of four steps. First step was the simulation of injection-moulding in order to provide orientation tensor of fibres distribution (FOD) all over the injected part. Second step was the estimation of the local effective properties of the composite material at any point, based on the orientation tensor and assuming, in the proposed extended version of the TPM, a viscoelastic matrix. Third step was to compute the mechanical response of the part (Abaqus®) over one cycle, for each applied load level. Fourth step was to calculate the Fatigue Indicator Parameter (FIP) for each load level and correlate it to the number-of-cycles-to-fracture via the fatigue criterion. This last step implied define the way how to apply the fatigue criterion, either very locally or over a larger volume. With the aim of making the approach usable in an industrial context, the

calculation chain was based on three different commercial software (Moldflow®, Digimat®, Abaqus®).

Four main challenges arose from the extension of the TPM to high-temperature with the aim to account for the viscoelasticity of the PA66 matrix. The first issue was the definition of the viscoelastic constitutive law of the polymer, which should be rather easy-to-use in an industrial context. The second issue was the choice of a new fatigue criterion to replace the elastic energy -based criterion used in the original methodology. The third issue was to define and simulate a stabilized cycle/state from which the FIP could be extracted and considered as representative of the major part of the material fatigue life. This question is not trivial for a material exhibiting a time-dependent mechanical behaviour.

The identification of the model parameters and the validation of the methodology relied on experimental fatigue data. Uniaxial tensile fatigue tests were carried out on dog-bone samples cut in injected plates of short glass fibres (30% in weight) reinforced PA66 (PA66GF30).

The experimental procedure and results are presented in section 2. Section 3 focuses on the development of the TPM methodology itself, considering the main challenges listed above. In section 4, the approach is applied to the experimental database constructed in section 2. The quality of the methodology in a viscoelastic framework at 110°C is presented and discussed. Improvement due to the introduction of viscoelasticity is evaluated from the comparison to results obtained with the previous elastic method.

2. Experimental

2.1 Material

The investigated material was a short glass fibre reinforced Polyamide 66 with a fibre content

of 30% by weight (PA66GF30), provided by Radici Plastics (Italy) as 3.3mm-thick injected plates. Glass fibres had a nominal diameter of 10µm and an average length of 275µm [21]. Their elastic behaviour was ruled by a Young's modulus equal to 72000 MPa and a Poisson ratio equal to 0.22 [6].

The PA66 matrix was a semi-crystalline thermoplastic with viscous mechanical properties, assumed to be viscoelastic in the present work. Details about modelling will be given in section 3.2. PA66 was known to be hydrophilic, with a related sensitivity of physical and mechanical properties to the relative humidity. In order to ensure repeatable state of samples before testing, they were conditioned in a dry-as-moulded state (DAM) in a hermetic chamber. The evolution of the weight of different specimens was measured and only a slight evolution was observed (weight gain of less than 0.3%). Anyway, the weight gain was stabilised before testing.

Injected plates exhibited a classical skin-core microstructure, with a core layer about 400µm-thick and two symmetrical 1.4mm-thick skin layers within which fibres were respectively mainly oriented perpendicularly and parallel to the injection direction. The dogbone specimens (see Fig. 1 for the dimensions**)** used for fatigue tests were cut out from the injected plates with 3 different angles θ to the injection direction: 0, 45 and 90°. Only one specimen was cut per plate in order to ensure the repeatability of the microstructure for the specimens oriented in the same direction. The position of each sample (illustrated in Fig. 1) was such that the central zone was far enough from the injection gate and from the plate sides.

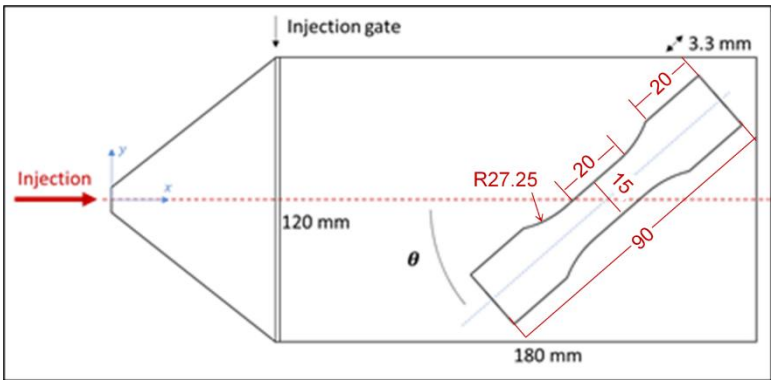

Fig. 1: Location, orientation and dimensions of the specimen cut out from each injected plate for fatigue tests.

2.2 Fatigue testing

Force-controlled fatigue tests were conducted in an INSTRON 8802 hydraulic fatigue machine, equipped with a climatic chamber. Temperature was regulated at 110°C ± 1°C. Prior to fatigue testing, the sample was taken out of the hermetic chamber inside which it was stored in a dry-as-moulded state (DAM) after injection-moulding. It was clamped and fitted with the extensometer. Then the temperature was raised from the ambient up to 110°C for 30 minutes and maintained at 110°C during 45 minutes more, in order to stabilise both the sample temperature and the thermal expansion of the device. The sample was thus considered to be still in a DAM state during testing. The sample was force-controlled at 1MPa during the temperature ramp and plateau.

Fatigue tests were conducted with a sinusoidal signal at constant frequency (2Hz to avoid self-heating) and stress amplitude. Two load ratios (defined as the ratio between the maximum applied stress and the minimum one) were considered: R = 0.1 and R = - 1. A guiding device was used in the latter case, in order to avoid buckling of the dogbone sample [6]. Samples were fitted with an extensometer to measure the macroscopic strain in the

loading direction. This was done for both tension and compression loadings. Samples tested at R = 0,1 were fitted with an INSTRON 2620-601 extensometer (12.5mm ±5 mm) on the front face (width of the sample). Due to the presence of the anti-buckling guiding device, samples tested at R = -1 were fitted with an INSTRON 2620-603 extensometer (10 mm ±1 mm) on their side surface (thickness of the sample).

2.3. Results

Fatigue tests were carried out with a double objective. On one hand, fatigue curves constituted the experimental database further used to identify the different parameters of the model and to validate the fatigue life estimation methodology. On the other hand, an analysis of the cyclic response was conducted to define the input stabilised cycle for the fatigue criterion and identify the constitutive law of the matrix.

a) Fatigue curves

Results in terms of amplitude loading Σ_a as a function of number of cycles to failure, N, are presented as S-N lines in Fig. 2, for the three orientations of samples and the two tested load ratios. The power interpolation lines were described by Basquin's law expressed in equation (1):

$$\Sigma_a = aN^{-b} \quad (1)$$

Only one test was conducted for each level of amplitude stress. However, the very good alignment of the points along the Basquin's lines suggested the low scatter usually observed in SFRT at room ([6], [10], [11], [16], [17]) but also at elevated temperature ([7], [10], [16], [17]).

For both R = 0.1 and R = -1, the resistance to fatigue classically increased with decreasing orientation angles. It resulted from the major alignment of fibres in the loading direction in the thick skin layer. As a proof of the mean stress effect, the resistance was lower for specimens tested at R = 0.1 than for specimens tested at R = -1. This was consistent with the literature either at room temperature ([6], [10], [16]) or at elevated temperature ([7], [16]).

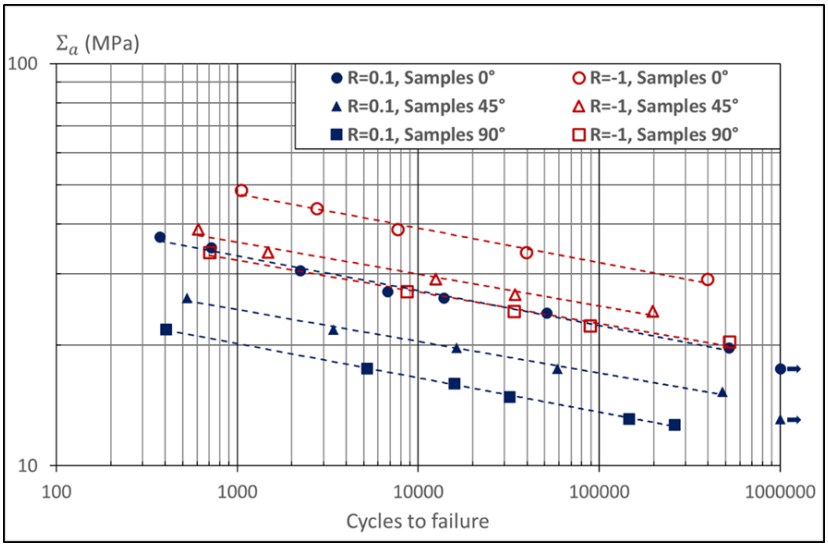

Fig. 2: S-N lines from uniaxial fatigue tests conducted at 110°C for three sample orientations (0, 45 and 90°) and two load ratios (R = 0.1 and R = -1).

b) Cyclic behaviour

In order to apply a fatigue criterion, the input mechanical quantity should be considered as stabilized at least, stationary. It was defined here by considering different parameters measured on the experimental stress Σ -strain e loops whose evolution was followed during the tests. These parameters were the hysteresis area, the secant modulus and the mean strain as defined in Fig. 3 for cycle *k*.

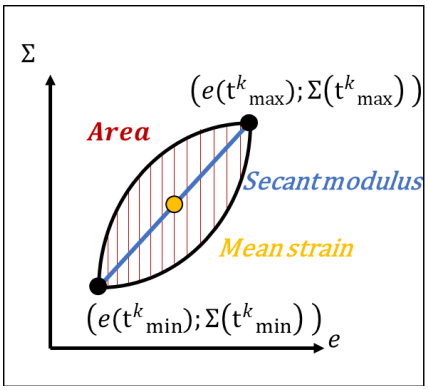

Fig. 3: Schematic representation of the stress-strain loop at cycle k and definition of the parameters associated with stabilization analysis: hysteresis area, secant modulus and mean strain.

The evolution of these parameters was tracked along fatigue tests. Only the evolution of the hysteresis area (linked to the FIP defined later) is represented in Fig. 4, for the three sample orientations (0, 45, and 90°) and the two tested load ratios (R = 0.1 and R = -1).

Curves globally displayed two or three main stages respectively, for tests at R=-1 and R=0.1. In the latter case, an initial transitory step was observed over the very first cycles. It could be explained both by the stabilisation of the force delivered by the hydraulic control and the fact that the stress-strain loops were not closed yet during the first cycles of testing (meaning that the first and last points of the cycle did not coincide). The second stage corresponded to the stabilisation of the hysteresis area and of the secant modulus (not represented here), especially for the tests leading to the longest fatigue lives. Such a stationary state was also observed for short fibre reinforced PA66 at ambient temperature by Jégou et al. [22] and Leveuf et al. [9]. The last stage corresponded to an important loss of stiffness and an important raise of the hysteresis area and the mean strain. This last step could be associated with the propagation of damage leading to the complete failure of the material.

From these observations, the 100th cycle of each curve was considered as representative of the stationary stage. This was particularly true for the longest fatigue lives for which the

stabilisation was clearer. Indeed, at the 100th cycle, the evolution rates of the loops parameters between two consecutive cycles did not exceed 0.3% except for two isolated curves corresponding to very low fatigue lives. Moreover, except the softening observed during the four first cycles, the parameters did slightly evolve at the 100th cycle and significantly evolved only in the last percent of the fatigue life (except for very low fatigue lives). This is consistent with a criterion-based design methodology for fatigue lives governed by initiation stage.

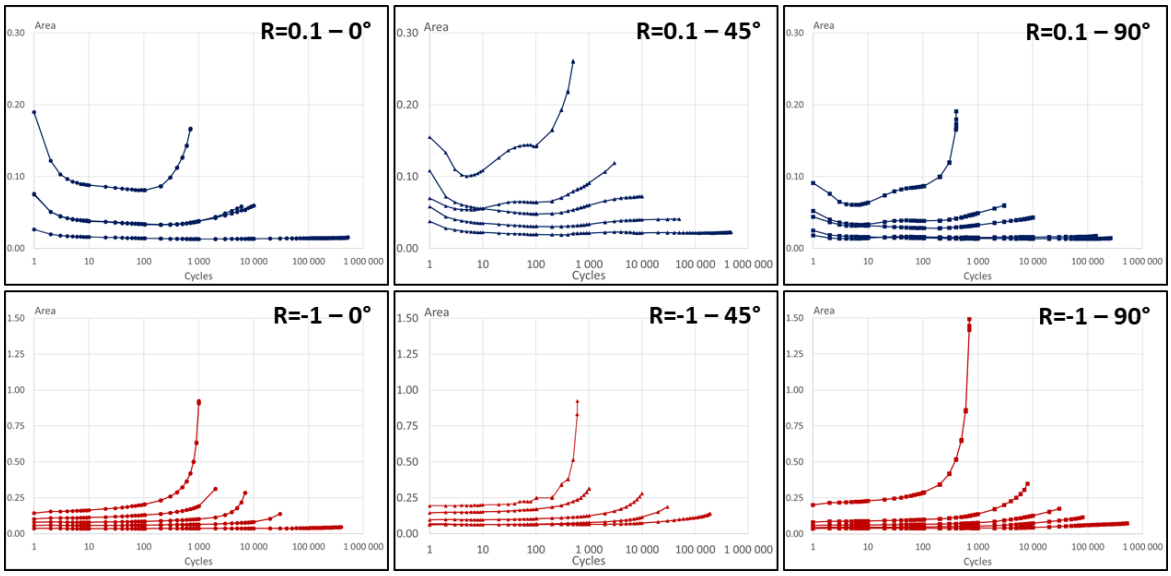

***Fig. 4*: Evolution of the hysteresis area during the fatigue life at 110°C for each tested sample**

3. Fatigue life assessment from TPM methodology

This section aims at presenting successive stages of the TPM with special focus on issues related to its extension to the viscoelastic framework.

3.1 Injection-moulding simulation

Injection-moulding was simulated with Moldflow® software. The output for the following stages of the TPM was a second-order orientation tensor at each integration point of the part.

The simulation giving this second-order orientation tensor needed two family of parameters. The first one was the injection parameters that were given by the material manufacturer. The second one was associated to equations related to the modelling of the fibres motion in a Newtonian flow taking into account the fibres-fibres interaction.

The models available in Moldflow® were the model of Folgar-Tucker [23] and the Reduced Strain Closure (RSC) model [24] (based on [25]). The associated equations were dependent on the fourth-order orientation tensor constructed from the second-order one with an hybrid closure approximation [26], [27]. The model used in the present work was the RSC model and needed two parameters, C_I and κ. The parameter C_I is called the interaction coefficient while $1/\kappa$ is the strain reduction factor. Their identification was done by comparing measurements of the principal components of the second-order orientation tensor and corresponding numerical predictions on different zones of the injected plates. Experimental observations were done by P. Hine (Leeds University, UK) following a methodology described in [28]. Special attention was paid to ensure the best agreement as possible between experimental values and predictions in the region from which samples were cut out (Fig.1). In this area, fibres were homogeneously oriented both in the skin and core layers, respectively in the injection direction and perpendicularly to it. In the first third of the plate, close to the gate, they were homogeneously oriented too in the skin layers but not in the core one. The values finally obtained were: $C_I = 0.009$, $\kappa = 0.41$.

3.2 Local mechanical properties estimates as a function of fibre orientation distribution

a) Orientation transfer - Viscoelastic homogenization

The second stage of the TPM was the estimate of the homogenized viscoelastic properties at

each point of the model used for FE analysis. Prior to this stage, the orientation tensor components had to be transferred from the Moldflow® model to the FE (Abaqus®) model. Digimat®-MAP software was used to this aim. The receiver mesh (Abaqus®) was generated with the same type of elements and average mesh size (1mm) as the donor mesh (Moldflow®). In order to optimize the quality of the transfer, special attention was paid to the region from which the samples were cut out. The aim was to have a regular mesh and identical to the donor one.

The viscoelastic homogenisation was processed with Digimat®-MF [29] according to a classical procedure. The linear viscoelastic heterogeneous problem was turned into a symbolic linear elastic problem by using the Laplace-Carson transform. This elastic problem was solved in the Laplace domain by a linear scheme before coming back to the real time domain using the collocation method. The linear homogenization model was based on the Mori-Tanaka scheme and on an orthotropic closure approximation to compute the fourth-order orientation tensor from the second-order one provided by the injection simulation. This procedure was linked to the viscoelastic FE simulation at each time step as explained in section 3.3.

The input data for viscoelastic homogenization were the properties of each phase (elastic glass fibres and viscoelastic PA66) and the morphological characteristics of the composite (i.e. the aspect ratio, volume ratio and local second-order orientation tensor of fibres at any point). They are detailed in the next sub-section.

b) Constituents properties

The properties for the glass fibres (Young's modulus E = 72000 MPa ; Poisson ratio ν = 0.22) were supposed identical at room temperature and at 110°C. They were issued from [6]. The

aspect ratio, calculated from the average length and diameter given in the work of Bernasconi et al. [11], was equal to 0.275. The volume ratio of fibres was deduced from the mass ratio, the density of glass (2540 kg/m3 [30]) and the density of PA66 (1360 kg/m^3 [5]).

The matrix was considered as linear viscoelastic and isotropic following the Prony series representation available in Digimat®. The shear and bulk relaxation moduli $G(\mathrm{t})$ and $K(\mathrm{t})$ were thus defined in the following way:

$$G(t) = G_0\left[1 - \sum_{i=1}^{n} g_i\left(1 - e^{-t/\tau_i}\right)\right], \qquad g_i = \frac{G_i}{G_0} \tag{2}$$

$$K(t) = K_0\left[1 - \sum_{i=1}^{n} k_i\left(1 - e^{-t/\tau_i^*}\right)\right], \qquad k_i = \frac{K_i}{K_0} \tag{3}$$

with G_0, K_0 the initial glassy moduli, g_i and k_i the shear and bulk weight factors, and G_i and K_i the shear and bulk moduli associated to relaxation times τ_i and τ_i^*, respectively. The number of relaxation times was not limited but in order to reduce calculation time, it had to be low.

It was well known that the behaviour of the thermoplastic polymer within the composite differed from that of the bulk polymer. Consequently, the identification of the matrix viscoelastic law relied on macroscopic data obtained from the testing of composite samples. This identification strategy was also designed in accordance with the choices made for further stages of the TPM. The FIP involved in the employed fatigue criterion (fourth stage of the TPM, section 3.4) was the dissipated energy over one cycle that should be representative of a stabilized, at least stationary, state. It has been observed (section 2.3-b) that the 100$^{\mathrm{th}}$ cycle could be considered as representative of a stationary cycle. However, and following the idea of Klimkeit et al. as a first attempt, the FIP was deliberately computed over the first closed cycle, corresponding to the second one. This choice was motivated by the industrial application context, requiring a minimum number of cycles to be simulated, and the expected inability of the viscoelastic framework to reproduce the composite cyclic behaviour until

stabilisation. To give more sense to this strong simplification, the matrix viscoelastic law was identified in such a way that the 2nd macroscopic simulated cycle coincides with the 100th experimental one. In some manner, this strategy led to the building of an "equivalent" composite whose second cycle was aimed to approach the 100th ("stabilized") cycle of the real composite. In such a strategy, it seemed reasonable to consider only three relaxation times for the matrix law which offered also the advantage to minimize the computational time.

Due to the lack of multiaxial tests, the difference between Prony parameters associated to shear and bulk moduli could not be documented. Thus, the relaxation times and weights were supposed to be the same for the bulk and shear moduli. Relaxation times were set within 2 decades centred on the duration of 1 loading cycle (0.5s at 2Hz). Initial values for the instantaneous and relaxed moduli were deduced from the 100th experimental cycle of the samples undergoing the highest and lowest strain rates. Then, the identification process was based on the samples exhibiting the two longest fatigue lives for each of the three orientations and each load ratio. More precisely, the identification was conducted by minimizing the relative error on macroscopic hysteresis area and secant modulus between the 100th experimental cycle and the 2nd simulated one for these twelve samples. The simulation was done using Digimat®-Abaqus® and the axial strain was deduced from the relative displacement of 2 nodes located as close as possible to the position of the two knives of the experimental extensometer. The macroscopic axial stress was calculated from the applied force divided by the initial cross-section area of the sample as for experiments.

Table 1 presents the parameters finally obtained.

	$G_0 = 226.5\ MPa$	$K_0 = 11250\ MPa$
$\tau_i = \tau_i^*$	g_i	k_i
0.05	0.156	0.156
0.5	0.0496	0.0496
5	0.0169	0.0169

Table 1: Parameters of the Prony series for the matrix viscoelastic law.

The relative error (defined as the difference between the numerical and the experimental values divided by the experimental one) fluctuated between 7 and 36% for the hysteresis area, and between 1 and 26% for the secant modulus. As an illustration of the quality of the identification, Fig 5 compares the 2nd macroscopic simulated cycle to the 100th experimental one in the best of the twelve situations regarding the relative error on the hysteresis area (7% at R = -1 and 90° in Fig. 5(a)) and the worst one (36% at R = -1 and 0° in Fig. 5(b)). As only 2 loading cycles were simulated, the mean strain evolution could not be considered directly. In these graphs, the mean strain was artificially shifted to make the comparison easier.

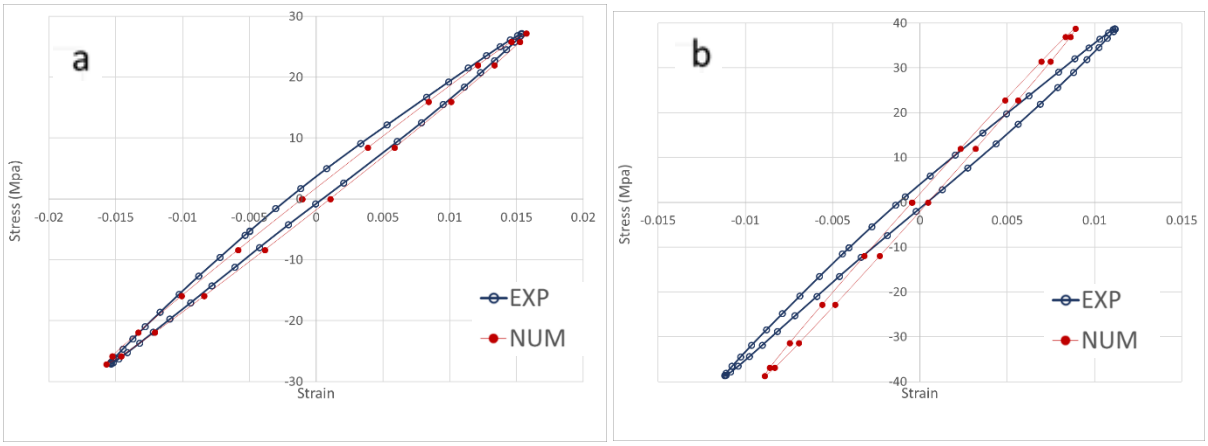

Fig. 5: Comparison between the 2nd macroscopic simulated cycle and the 100th experimental cycle. a: sample oriented at 90° - R = -1. b: sample oriented at 0° - R = -1.

3.3 Finite Element Analysis

The FE analysis was performed with Abaqus® using a Digimat® plugin giving the local homogenised mechanical properties at each time step of loading. The sample was meshed with 2D triangular shell elements S3, divided into 20 layers through the thickness of the sample, with three integration points (IP) in each layer. For each layer of each element, the corresponding fibre orientation tensor was attached. This means that the same orientation tensor was attached to the three IP of each layer of an element. In the sample plane, the mesh size was set at 1mm, for matching purpose with the injection-moulding simulation with Moldflow® and thus minimize the interpolation error during the transfer of the orientation tensor. For the same reason, the triangular shape of the elements matched the Moldflow® model.

The FE simulations were conducted with the same loading profile (sinusoidal wave form, frequency, maximal applied load, load ratio,…) and boundary conditions as the experiments. As explained above, only two cycles were simulated. The load was applied to a single node of the lower head of the sample, tied to all the nodes in the head; only translation in the direction of loading was allowed. The upper head was clamped and thus fully constrained (6 degrees of freedom were locked).

3.4 Fatigue criterion

a) Formulation and FIP calculation

Assuming that the dissipated energy was the mechanical quantity monitoring the fatigue life, the criterion of Jegou et al. [22] was selected. It was written as follows:

$$\Delta^* = CN^{-b} \quad (4)$$

with Δ^* the dissipated energy over one cycle (that should be stabilized), N the number of cycles to failure and b and C two material parameters. As previously done by Klimkeit et al. [6] for the elastic energy-based criterion, a specific parameter f was added to take into account the mean stress effect. This parameter was calculated from the solving of an empirical equation proposed by Kujawski and Ellyin [31]:

$$f^2 - \frac{\sigma_m}{\sigma_a} f - 1 = 0 \quad (5)$$

where σ_m and σ_a are respectively the mean and amplitude stresses characterizing the macroscopic fatigue loading. The positive solution of the previous equation was taken and the fatigue criterion became:

$$f\Delta^* = CN^{-b} \quad (6)$$

The input mechanical quantity (FIP) for the fatigue criterion was thus $f\Delta^*$. f was given by solving equation (5) and only depended on the macroscopic load ratio while Δ^* had to be evaluated from the post-processing of the FE analysis. The dissipated energy per unit volume over one cycle was here assimilated to the mechanical energy received over the cycle (nullity of the stored energy). In the particular case of a uniaxial stress state, this would have consisted in assimilating the dissipated energy over the cycle to the hysteresis area of the axial stress-strain response as commonly done in the literature. It must be reminded that local stress state within a sample, even under uniaxial macroscopic loading, is potentially multiaxial due to the local fibre orientation distribution and specimen geometry. This is even truer for injected parts with complex geometry.

In this paper, as a first approach devoted to uncouple the different effects, the application method of the fatigue criterion, for both its identification and further validation of the whole TPM, followed the same principle as the one proposed by Klimkeit et al. [6]. The local dissipated energy over the second simulated cycle, assimilated to the received mechanical energy, was indeed averaged over the volume of each element of the specimen. Then, Δ^*, used as input for the criterion, was the maximum value obtained over all the elements of the model:

$$\Delta^* = \mathrm{Max}_{elements}\langle D\rangle_{V_e} \qquad \text{with} \qquad D = \oint_{\text{2nd cycle}} \bar{\bar{\sigma}} : \dot{\bar{\bar{\epsilon}}}\, dt \tag{7}$$

A Python scrypt has been specifically developed in order to compute (i) the received energy over the second cycle at each integration point, then (ii) the average over the volume of each element and (iii) finally the search of the maximum value within the part and corresponding element.

b) Identification of the criterion parameters

The fatigue criterion (equation (6)) required one S-N line for the identification of both material parameters *C* and *b*. Following the previous work in elasticity [6], the S-N line of the specimens oriented at 0° and loaded at R = -1 was chosen. The mean stress correction via *f* was thus inactive (*f =1* according to equation (5)).

The TPM was applied to the selected specimen (0° orientation) for all the stress levels of the experimental S-N line. Then, the FIP, Δ^*, calculated according to the foregoing methodology (section 3.4-a), was plotted against the experimental number of cycles to failure (in log-log scale). The interpolation equation directly provided the parameters *C* and *b* of the fatigue criterion: *C* = 0.346 and *b* = 0.171. The influence of the S-N line chosen for the identification of the fatigue criterion will be discussed in the next section.

4. Results and discussion

The TPM has been applied to every specimen and loading condition of the whole database available at 110°C. Results are presented in the following with two angles, the prediction of the locations of fatigue failure and the prediction of the fatigue lives.

4.1 Failure initiation location

The post-process of mechanical fields, as described in section 3.4-a, allowed to get the average received mechanical energy in each element of a loaded specimen and to identify the element exhibiting the maximal value. Fig. 6 and Fig. 7 display maps of the average energy for R = 0.1 and R = -1 respectively, at stress levels leading to the longest lifetime for each of the three fibre orientations. Maxima are marked with blue dots.

In all cases, "hot points" were located in the fillets of the specimens. For the specimens oriented at 0° and 90°, the 4 filets were hot points. However, gradients were stronger for the 0° sample than for the 90° one. In the latter case, the fatigue indicator was more homogeneous within the gauge length. Due to the fibre orientation in specimens at 45°, only the top right and bottom left fillets were hot points. The combined effects of fibre orientation and geometry of the specimen led to higher stress concentration at these points. The effect of the load ratio was mainly related to the values of energy reached: at R = 0.1, maximal stresses were higher than those obtained at R = -1.

Fig. 8 displays views of samples broken after testing at R = 0.1 and R = -1 and exhibiting the longest fatigue lives for each orientation. Most of the specimens failed in the fillets (top or bottom) except samples oriented at 90° and tested at R = 0.1 that failed in the middle. It could

be related to the weaker heterogeneity of the average energy in these samples, as evidenced from the FE simulation in Fig.6. Indeed, when gradients are weaker, other potential sources of experimental variability may better express and lead to the failure.

The comparison between experiment and simulation showed that this energy could be a good driving parameter to predict the location of the less resistant areas to fatigue loading.

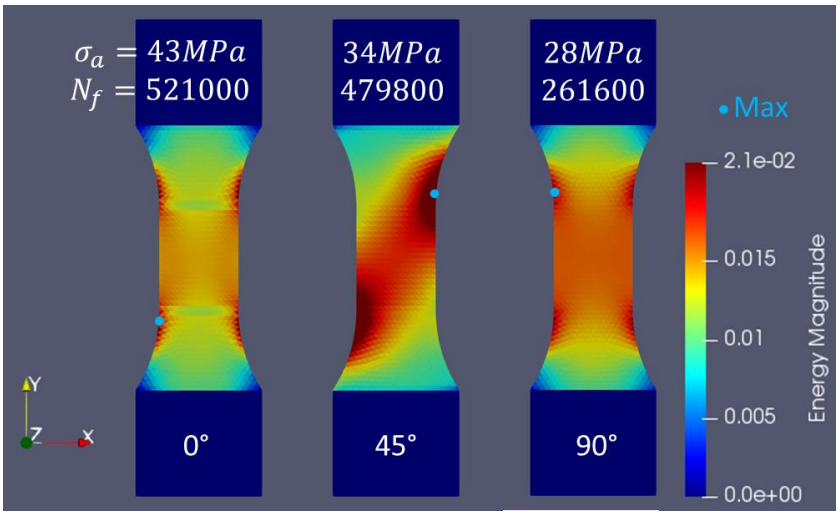

Fig. 6: Mapping of the simulated energy (averaged over the volume of each element) for three specimens (0, 45 and 90°) tested at R = 0.1 and exhibiting the longest fatigue life. The element displaying the maximum of average energy (mJ/mm^3) is marked with blue dot.

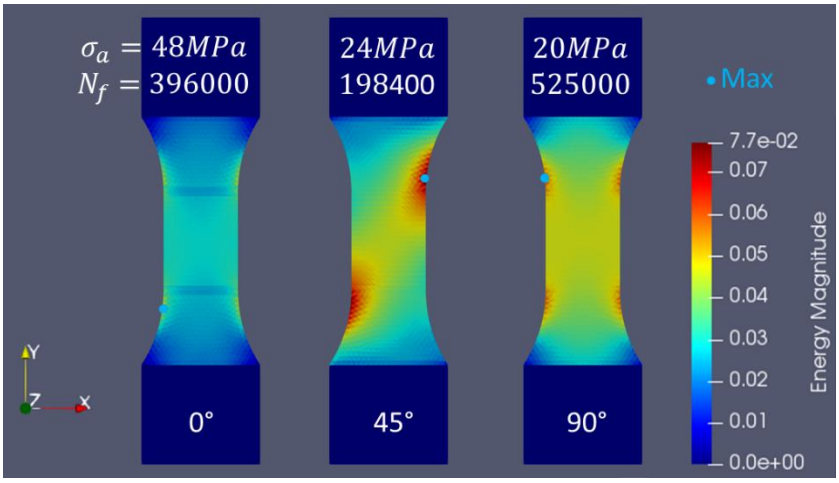

Fig. 7: Mapping of the simulated energy (averaged over the volume of each element) for three specimens (0, 45 and 90°) tested at R = -1 and exhibiting the longest fatigue life. The element displaying the maximum of average energy (mJ/mm^3) is marked with blue dot.

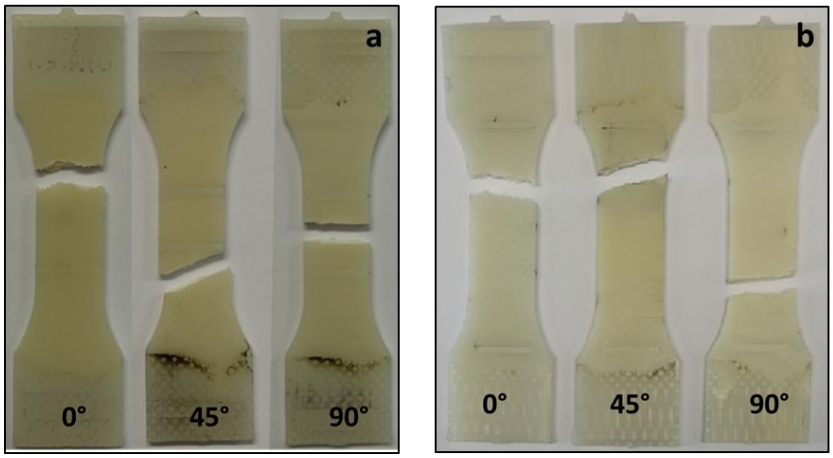

Fig. 8: Failure locations of samples tested at (a) R = 0.1 and (b) R = -1 and exhibiting the longest fatigue life.

4.2 Comparison of experimental and simulated fatigue lives

For each sample and loading condition, the knowledge of the maximal value Δ^* of the average energy over all the elements of the sample allowed estimating the simulated number of cycles to failure $N_{calculated}$ as follows:

$$N_{calculated} = \exp\left(\frac{\ln(C) - \ln(f\Delta^*)}{b}\right) \quad (8)$$

where f was deduced by solving equation (5) for the load ratio considered and, b and C were identified by applying the TPM to the samples with 0° orientation, tested at R=-1 and using the corresponding S-N line (see section 3.4-b). The number of cycles $N_{calculated}$ was compared to the number of cycles to failure experimentally obtained ($N_{experimental}$). Results are shown in Fig 9. The perfect prediction is the line driven by the equation $N_{calculated} = N_{experimental}$. This line is the limit between conservative results

($N_{calculated} < N_{experimental}$) and non-conservative results ($N_{calculated} > N_{experimental}$). The thin dashed lines represent a difference of + or – 1 decade with the perfect prediction line while the thick dashed lines correspond to a difference of + or – 2 decades.

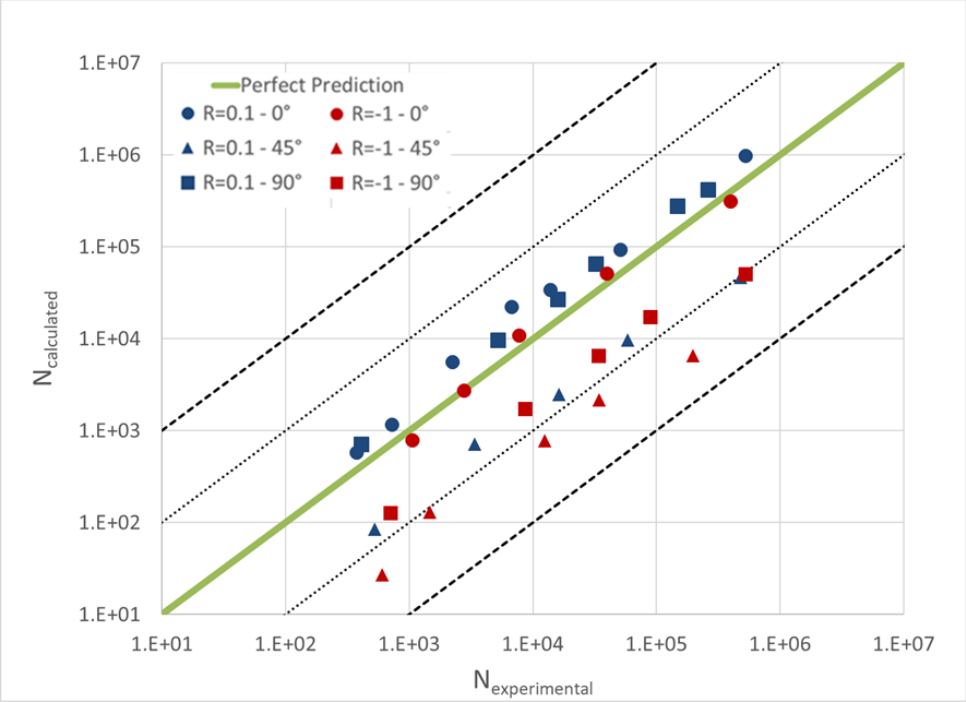

Fig. 9: Results of the fatigue life assessment methodology (TPM) at 110° C in the viscoelastic framework: simulated against experimental numbers of cycles to failure.

For each orientation and load ratio, results were either conservative (in the limit of 1 decade except for the samples oriented at 45° and tested at $R = -1$) or very close to the perfect prediction (in the limit of +1 decade for the samples oriented at 0° and 90° and tested at $R = 0.1$).

In order to quantify the benefit of the viscoelastic framework compared to the elastic one, the TPM in its elastic version due to Klimkeit et al. [6] has been applied to the whole database at 110°C. The same fibre orientation distribution was used for FE analysis. Elastic properties at 110°C of the PA66 matrix, issued from the supplier, were: E = 530MPa, ν = 0.49, while the properties of the fibres were unchanged. The Mori-Takana scheme and the same closure

approximation as in section 3.2-a were employed for the elastic homogenization. At last, the fatigue criterion, (equation (6)) with the elastic energy replacing the dissipated energy, was applied with the same averaging process (volume average of the energy over each element and search for the maximum value). Using the same S-N line and procedure as in section 3.4-b, the parameters of the elastic energy-based fatigue criterion were obtained: C = 1.532 and b = 0.171. Simulated fatigue lives finally obtained with the elastic TPM are plotted as functions of the experimental values in Fig. 10. Prediction were particularly poor at R = 0.1 with a difference to the perfect prediction larger than 3 decades (against 1 with the extended, viscoelastic, TPM). More generally, results obtained for the 3 orientations and 2 load ratios were better unified in the viscoelastic framework (Fig. 9) than in the elastic one (Fig. 10).

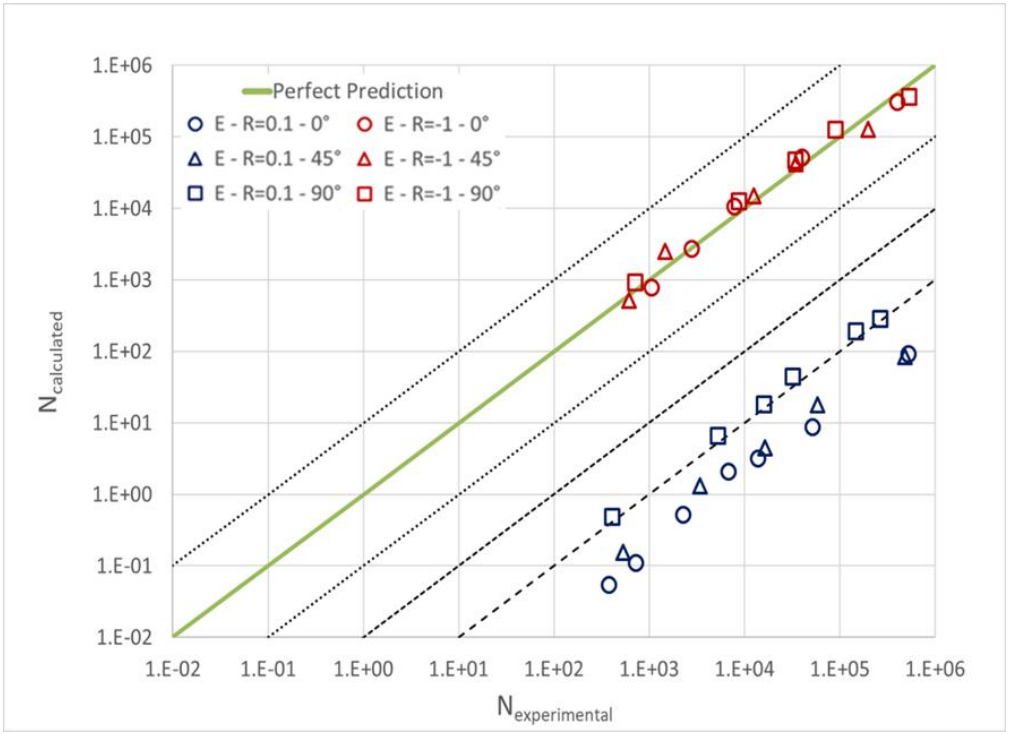

Fig. 10 : Results of the fatigue life assessment methodology (TPM) at 110° C in the elastic framework: simulated against experimental numbers of cycles to failure.

In the following, a discussion is proposed regarding two issues. The first one is related to the fatigue criterion (mean stress correction and parameters identification) and the second one

regards the matrix viscoelastic law.

Regarding the first point, Fig. 11 shows the predictions obtained with the viscoelastic TPM by applying the fatigue criterion without mean stress correction, equation (4). It must be noted that the criterion parameters, previously identified in section 3.4-b on specimens oriented at 0° and loaded at R = -1, were unchanged. The comparison between Fig. 11 and Fig. 9 clearly illustrates the improvement provided by the empirical mean stress correction due to [31], as previously observed in elasticity by Klimkeit et al. [6]. Predictions obtained at R= 0.1 with mean stress correction (Fig. 9) are much better and the difference between the results obtained for both load ratios is reduced. However, some work is still necessary to enhance the description of the mean stress effect.

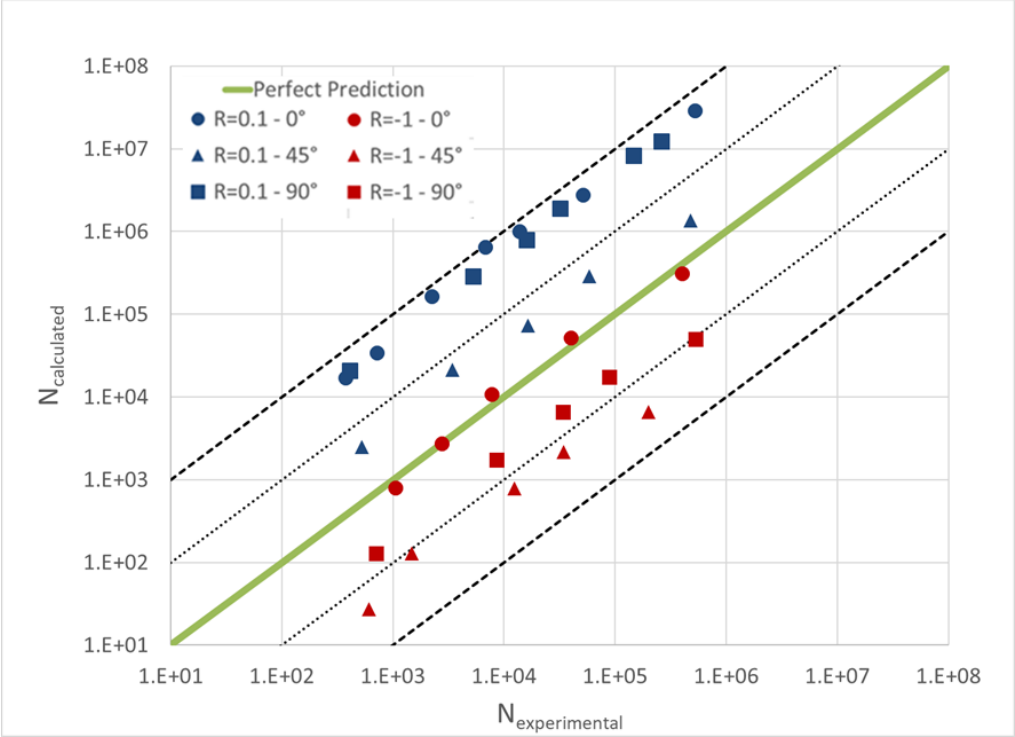

Fig. 11: Results of the fatigue life assessment methodology (TPM) at 110°C in the viscoelastic framework without mean stress correction: simulated against experimental number of cycles to failure.

In order to appreciate the influence of the S-N line chosen for the criterion identification, Fig. 12 plots the simulated FIP, $f\Delta^*$, against the experimental number of cycles to failure for all the

loading conditions and specimen orientations. The lines are the power interpolations for each specimen orientation and load ratio, from which the criterion parameters b and C could be identified. In the foregoing (section 3.4-b), the line corresponding to the specimens with 0° orientation loaded at R = -1 was chosen for the criterion identification. As shown in Fig. 12, every curve displayed the same slope (parameter b), only the level of energy differs (parameter C). Since the slope is the same, choosing one curve or another to identify the criterion parameters would only lead to a translation of the predicted fatigue lives. The scatter as well as the orientation and mean stress effects would stay the same than in Fig. 9. The choice of the specimens oriented at 0° for a load ratio of R = -1 led to get most of the results within a limit of 1 decade from the perfect prediction. Even if some predictions were slightly non-conservative, this choice appeared as relevant. An identification from the experimental S-N line 0°/R = 0.1 would translate the points down in Fig. 9. All the results would be conservative but with a strong underestimation of the fatigue lives of the specimens 45° - 90°/R = -1.

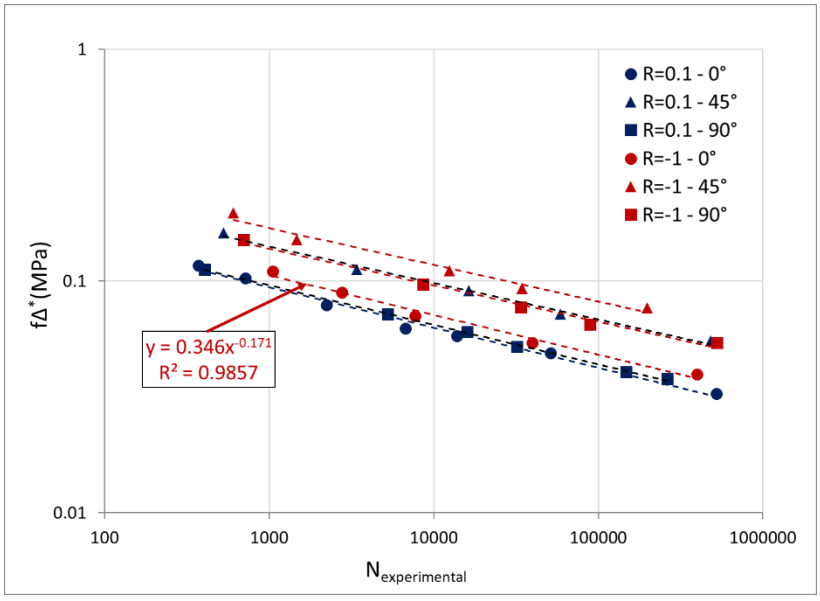

Fig. 12: Simulated FIP as a function of the experimental number of cycles to failure.

At last, improvement of the present methodology could arise from a better identification of the constitutive law of the matrix. As a first step, the numerical identification itself could be optimized. More generally, in accordance with fundamental knowledge of polymer viscoelasticity, relaxation times should be differentiated for the bulk and shear generalized moduli in the Prony series. To this aim, fatigue tests along other loading paths, like shear tests, should be included to the database.

Nevertheless, since the matrix viscoelastic law was extracted from a micromechanical analysis of the composite behaviour, it was never identified from pure uniaxial loading, even from a basic macroscopic tensile test. Identification from tensile tests already resulted from a compromise between various local states in the matrix, due to the local disorientation of fibres. But, by integrating shear or fatigue tests to the database for the constitutive law of the matrix, a broader set of multiaxial states would be accessible and make possible a separate identification of bulk and shear relaxation times. At last, some fatigue data involving negative load ratios should also be added.

5. Conclusion

The main goal of this study was to integrate the viscoelastic behaviour of the PA66 matrix in a through-process modelling method for fatigue life estimation of Short Fibre Reinforced Thermoplastics at high temperature. In order to keep a rather easy-to-use method for industrial components, the method was based on a chain of commercial softwares (MoldFlow®, Digimat® and Abaqus®).

The fatigue test database was obtained from tensile tests in PA66GF30 dogbone specimens machined out from injection-moulded plates, with three different orientations to the injection direction: 0, 45 and 90°. Force-controlled fatigue test were performed at 110°C in Dry-As-Moulded specimens, under constant amplitude and frequency (2Hz) and two load ratios (0.1 and -1).

At any point of the sample, the anisotropic viscoelastic response was estimated (Abaqus® software coupled to a Digimat® plug-in) from a micromechanical calculation based on the morphology of the composite, the fibres elastic behaviour and the matrix viscoelastic one. The orientation tensor of fibres was transferred from MoldFlow® simulation of injection-moulding. A systematic analysis of the stabilization of the macroscopic experimental stress-strain loop showed that a stationary state was reached after 100 cycles for all tests in the database. Therefore, the PA66 matrix viscoelastic law (expressed via Prony series on the bulk and shear moduli) was identified so that the second macroscopic simulated cycle corresponded to the stabilized one. The number of relaxation times could then be reduced to three. The Fatigue Indicator Parameter (FIP), chosen as the dissipated energy (assimilated to the received energy) over the stabilized cycle, was computed at any integration point using the local three-dimensional strain and stress tensors over this cycle, and averaged over the thickness of each element. The resulting maximum value of the FIP over all the elements was the input quantity of the fatigue criterion, expressed as a power law of the number-of-cycles-to-failure.

Maps of the FIP showed that the critical zones were located in the fillets of the specimen, as observed experimentally. The predicted number-of-cycles-to-failure were compared to the experimental ones. Results were close within one decade to the perfect prediction. It was shown that the introduction of viscoelasticity significantly improved the quality of predictions, compared to results obtained from the similar approach in a purely elastic framework. This is a noticeable result that could be improved now from a better calibration of the matrix constitutive law. The fatigue criterion itself should be reconsidered also to better capture mean stress effect. The mean stress correction model proposed by Eftekhari and Fatemi [32] could be used to this aim. Investigation on the application method of the criterion is under progress in the case of macroscopic singularities like notches or ribs.

Acknowledgements

Direction Générale de l'Armement (convention DGA n°3014.60.0058) and Région Poitou-Charentes are gratefully acknowledged for the PhD grant of Nathan Fouchier. Dr Irène Maillet and Dr Matthieu Guehenec from DGA are gratefully acknowledged for fruitful discussions. Computations have been performed on the supercomputer facilities of the Mesocentre de calcul SPIN Poitou- Charentes. Experiments were partly supported by funding from the European Community (FEDER FSE project HYGROPOLYM ref P-2017-BAFE-117).

References

[1] N. Despringre, Y. Chemisky, K. Bonnay, and F. Meraghni, 'Micromechanical modeling of damage and load transfer in particulate composites with partially debonded interface', *Composite Structures*, vol. 155, no. Supplement C, pp. 77–88, Nov. 2016.

[2] A. Krairi, I. Doghri, and G. Robert, 'Multiscale high cycle fatigue models for neat and short fiber reinforced thermoplastic polymers', *International Journal of Fatigue*, vol. 92, no. Part 1, pp. 179–192, Nov. 2016.

[3] H. Nouri, F. Meraghni, and P. Lory, 'Fatigue damage model for injection-molded short glass fibre reinforced thermoplastics', *International Journal of Fatigue*, vol. 31, no. 5, pp. 934–942, May 2009.

[4] S. Kammoun, I. Doghri, L. Brassart, and L. Delannay, 'Micromechanical modeling of the progressive failure in short glass–fiber reinforced thermoplastics – First Pseudo-Grain Damage model', *Composites Part A: Applied Science and Manufacturing*, vol. 73, no. Supplement C, pp. 166–175, Jun. 2015.

[5] A. Launay, M. H. Maitournam, Y. Marco, and I. Raoult, 'Multiaxial fatigue models for

short glass fibre reinforced polyamide. Part II: Fatigue life estimation', *International Journal of Fatigue*, vol. 47, no. Supplement C, pp. 390–406, Feb. 2013.

[6] B. Klimkeit *et al.*, 'Multiaxial fatigue life assessment for reinforced polymers', *International Journal of Fatigue*, vol. 33, no. 6, pp. 766–780, Jun. 2011.

[7] C. M. Sonsino and E. Moosbrugger, 'Fatigue design of highly loaded short-glass-fibre reinforced polyamide parts in engine compartments', *International Journal of Fatigue*, vol. 30, no. 7, pp. 1279–1288, Jul. 2008.

[8] A. Wilmes and K. Hornberger, 'Influence of Fiber Orientation and Multiaxiality on the Fatigue Strength of Unnotched Specimens – Lifetime Estimation', *Procedia Engineering*, vol. 133, pp. 148–160, Jan. 2015.

[9] L. Leveuf, Y. Marco, V. Le Saux, L. Navrátil, S. Leclercq, and J. Olhagaray, 'Fast screening of the fatigue properties of thermoplastics reinforced with short carbon fibers based on thermal measurements', *Polymer Testing*, vol. 68, pp. 19–26, Jul. 2018.

[10] S. Mortazavian and A. Fatemi, 'Fatigue behavior and modeling of short fiber reinforced polymer composites including anisotropy and temperature effects', *International Journal of Fatigue*, vol. 77, no. Supplement C, pp. 12–27, Aug. 2015.

[11] A. Bernasconi, P. Davoli, A. Basile, and A. Filippi, 'Effect of fibre orientation on the fatigue behaviour of a short glass fibre reinforced polyamide-6', *International Journal of Fatigue*, vol. 29, no. 2, pp. 199–208, Feb. 2007.

[12] Y. Zhou and P. K. Mallick, 'Fatigue Performance of an Injection-Molded Short E-Glass Fiber-Reinforced Polyamide 6,6. I. Effects of Orientation, Holes, and Weld Line', 2006.

[13] M. De Monte, E. Moosbrugger, K. Jaschek, and M. Quaresimin, 'Multiaxial fatigue of a short glass fibre reinforced polyamide 6.6 – Fatigue and fracture behaviour', *International Journal of Fatigue*, vol. 32, no. 1, pp. 17–28, Jan. 2010.

[14] K. Noda, A. Takahara, and T. Kajiyama, 'Fatigue failure mechanisms of short glass-

fiber reinforced nylon 66 based on nonlinear dynamic viscoelastic measurement', *Polymer*, vol. 42, no. 13, pp. 5803–5811, Jun. 2001.

[15] A. Benaarbia, A. Chrysochoos, and G. Robert, 'Thermomechanical behavior of PA6.6 composites subjected to low cycle fatigue', *Composites Part B: Engineering*, vol. 76, no. Supplement C, pp. 52–64, Jul. 2015.

[16] A. Launay, Y. Marco, M. H. Maitournam, and I. Raoult, 'Modelling the influence of temperature and relative humidity on the time-dependent mechanical behaviour of a short glass fibre reinforced polyamide', *Mechanics of Materials*, vol. 56, no. Supplement C, pp. 1–10, Jan. 2013.

[17] S. Barbouchi, 'Effect of water on the fatigue behaviour of a pa66/glass fibers composite material', *Journal of Materials Science*, vol. 42, no. 6, pp. 2181–2188, 2007.

[18] A. Launay, M. H. Maitournam, Y. Marco, and I. Raoult, 'Multiaxial fatigue models for short glass fiber reinforced polyamide – Part I: Nonlinear anisotropic constitutive behavior for cyclic response', *International Journal of Fatigue*, vol. 47, no. Supplement C, pp. 382–389, Feb. 2013.

[19] Y. Marco *et al.*, 'Dissipation analysis in SFRP structural samples: Thermomechanical analysis and comparison to numerical simulations', *International Journal of Fatigue*, vol. 67, no. Supplement C, pp. 142–150, Oct. 2014.

[20] A. Selmi, I. Doghri, and L. Adam, 'Micromechanical simulations of biaxial yield, hardening and plastic flow in short glass fiber reinforced polyamide', *International Journal of Mechanical Sciences*, vol. 53, no. 9, pp. 696–706, Sep. 2011.

[21] A. Bernasconi, D. Rossin, and C. Armanni, 'Analysis of the effect of mechanical recycling upon tensile strength of a short glass fibre reinforced polyamide 6,6', *Engineering Fracture Mechanics*, vol. 74, no. 4, pp. 627–641, Mar. 2007.

[22] L. Jégou, Y. Marco, V. Le Saux, and S. Calloch, 'Fast prediction of the Wöhler curve

from heat build-up measurements on Short Fiber Reinforced Plastic', *International Journal of Fatigue*, vol. 47, no. Supplement C, pp. 259–267, Feb. 2013.

[23] F. Folgar and C. L. Tucker, 'Orientation Behavior of Fibers in Concentrated Suspensions', *Journal of Reinforced Plastics and Composites*, vol. 3, no. 2, pp. 98–119, Apr. 1984.

[24] J. Wang, J. F. O'Gara, and C. L. Tucker, 'An objective model for slow orientation kinetics in concentrated fiber suspensions: Theory and rheological evidence', *Journal of Rheology*, vol. 52, no. 5, pp. 1179–1200, Sep. 2008.

[25] G. B. Jeffery, 'The motion of ellipsoidal particles immersed in a viscous fluid', *Proc. R. Soc. Lond. A*, vol. 102, no. 715, pp. 161–179, Nov. 1922.

[26] Moldflow, 'Moldflow's fiber orientation models (Theory), Moldflow Flex 2016, Autodesk Knowledge Network', 2018. [Online]. Available: https://knowledge.autodesk.com/support/moldflow-flex/learn-explore/caas/CloudHelp/cloudhelp/2016/ENU/MoldflowInsight360/files/GUID-6B3A7386-DE57-450E-BF94-B10BD629EC9B-htm.html. [Accessed: 07-Oct-2018].

[27] S. G. Advani and C. L. Tucker, 'Closure approximations for three-dimensional structure tensors', *Journal of Rheology*, vol. 34, no. 3, pp. 367–386, Apr. 1990.

[28] P. J. Hine, N. Davidson, R. A. Duckett, and I. M. Ward, 'Measuring the fibre orientation and modelling the elastic properties of injection-moulded long-glass-fibre-reinforced nylon', *Composites Science and Technology*, vol. 53, no. 2, pp. 125–131, Jan. 1995.

[29] Digimat, *Digimat - User's Manual - v2016*. 2016.

[30] B. Klimkeit, 'Etude expérimentale et modélisation du comportement en fatigue multiaxiale d'un polymère renforcé pour application automobile', PhD. thesis, ENSMA, 2009.

[31] D. Kujawski and F. Ellyin, 'A unified approach to mean stress effect on fatigue

threshold conditions', *International Journal of Fatigue*, vol. 17, no. 2, pp. 101–106, Feb. 1995.

[32] M. Eftekhari and A. Fatemi, 'Fatigue behaviour and modelling of talc-filled and short glass fibre reinforced thermoplastics, including temperature and mean stress effects', *Fatigue & Fracture of Engineering Materials & Structures*, vol. 40, pp.333–348, 2017.

Fatigue life assessment of a Short Fibre Reinforced Thermoplastic at high temperature using a Through Process Modelling in a viscoelastic framework

Nathan Fouchier[1], Carole Nadot-Martin[1*], Edoardo Conrado[2], Andrea Bernasconi[2], Sylvie Castagnet[1]

[1]Institut Pprime (UPR 3346 CNRS – ISAE-ENSMA – University of Poitiers), Department of Physics and Mechanics of Materials, Poitiers, France

[2] Politecnico di Milano, Dipartimento di Meccanica, Milano, Italie

* Corresponding author: carole.nadot@ensma.fr

Abstract: A Through Process Modelling (TPM) fatigue life assessment methodology – previously validated in an elastic framework for Short Fibre Reinforced Thermoplastics at room temperature– was extended to high temperature. The viscoelasticity of the matrix was taken into account to estimate the local effective mechanical properties at any point, from the knowledge of local fibre orientation provided by the simulation of injection-moulding. Lifetime estimation was obtained from an energetic fatigue criterion applied in the stationary regime. The approach was validated from uniaxial fatigue tests conducted at 110°C in tension, in PA66GF30 samples cut out from injected plates with three different orientations to the injection direction, at two stress ratios (0.1 and -1).

Keywords: PA66GF30; Viscoelasticity; Through Process Modelling; Homogenization; Energetic fatigue criterion.

1. Introduction

The use of composite materials as replacement of metallic alloys has been growing in automotive and aeronautic industry. Injection-moulded Short Fibre Reinforced Thermoplastics

(SFRT) and especially reinforced Polyamides have been widely used for structural parts.

The industrial design of parts requires numerical tools to assess their fatigue life under operating conditions. Different types of design methodology exist in the literature. Two main families could be distinguished. In approaches based on *non-linear constitutive laws*, the cyclic behaviour was continuously described using an evolution law of damage, for all or part of fatigue life [1-4]. This kind of approach was explicit but expensive regarding calculation and identification times. On the other hand, *fatigue-criterion* approaches directly connected a Fatigue Indicator Parameter (FIP) –calculated from the mechanical response over a stabilized cycle– to the number of cycles to failure. Damage evolution was not explicitly depicted; the challenge was to capture the key factors governing fatigue life into the FIP and the fatigue criterion equation. Such approaches were suitable when crack initiation occurred over a major part of the lifetime. Different criteria were proposed in the literature, based on equivalent stresses [5–8] or energy [5, 6, 9]. For this type of materials and at ambient temperature, the most recent works suggested to opt for energy-based criteria [5, 6].

Fatigue-criterion approaches have been widely used in industrial context, due to the possibly reduced calculation and identification time. In order to apply the fatigue criterion, the FIP should be calculated over a stabilised cycle or at least over a cycle on which it is stabilised. The cyclic behaviour and the fatigue strength of SFRT widely depended on the fibres orientation distribution (FOD) that was locally heterogeneous in an injected part [6], [8], [10]–[12], on the environment conditions, i.e. temperature ([7], [10], [13], [14]) and, in the case of hydrophilic polymers like polyamides, on the moisture content that plays a similar role ([10], [15]–[17]). The environment effect could be taken into account through the gap of temperature between the operating and glass transition ones [16]. Gathering all these influence factors (viscoelasticity, viscoplasticity, anisotropy, multi-physical coupling) into a constitutive law is still an open issue. Thus, most of modellings employed as input calculations for fatigue-

criterion approaches only retained some of them. Heterogeneity of fibre orientation and induced anisotropy should be a priority. In the literature, both phenomenological [18], [19] and micromechanical descriptions [6], [20] were used to this aim.

Because of the few experimental tests performed at higher temperature, most of the fatigue design model were proposed at room temperature. But the trend to use injected parts close to hot zones has been requiring the development of a life assessment tool suitable for higher temperatures.

This was the main objective of the present work. A Through Process Modelling (TPM) for fatigue life assessment of SFRT was developed for a polyamide-based composite (PA66GF30) at 110°C. The approach was extended from the TPM initially developed by Klimkeit et al. [6], validated for several SFRT at room temperature considering an elastic behaviour of the matrix. It was a fully integrated numerical approach linking the injection simulation to the estimate of the fatigue life. The TPM methodology was made of four steps. First step was the simulation of injection-moulding in order to provide orientation tensor of fibres distribution (FOD) all over the injected part. Second step was the estimation of the local effective properties of the composite material at any point, based on the orientation tensor and assuming, in the proposed extended version of the TPM, a viscoelastic matrix. Third step was to compute the mechanical response of the part (Abaqus®) over one cycle, for each applied load level. Fourth step was to calculate the Fatigue Indicator Parameter (FIP) for each load level and correlate it to the number-of-cycles-to-fracture via the fatigue criterion. This last step implied define the way how to apply the fatigue criterion, either very locally or over a larger volume. With the aim of making the approach usable in an industrial context, the calculation chain was based on three different commercial software (Moldflow®, Digimat®, Abaqus®).

Four main challenges arose from the extension of the TPM to high-temperature with the aim to account for the viscoelasticity of the PA66 matrix. The first issue was the definition of the

viscoelastic constitutive law of the polymer, which should be rather easy-to-use in an industrial context. The second issue was the choice of a new fatigue criterion to replace the elastic energy -based criterion used in the original methodology. The third issue was to define and simulate a stabilized cycle/state from which the FIP could be extracted and considered as representative of the major part of the material fatigue life. This question is not trivial for a material exhibiting a time-dependent mechanical behaviour.

The identification of the model parameters and the validation of the methodology relied on experimental fatigue data. Uniaxial tensile fatigue tests were carried out on dog-bone samples cut in injected plates of short glass fibres (30% in weight) reinforced PA66 (PA66GF30).

The experimental procedure and results are presented in section 2. Section 3 focuses on the development of the TPM methodology itself, considering the main challenges listed above. In section 4, the approach is applied to the experimental database constructed in section 2. The quality of the methodology in a viscoelastic framework at 110°C is presented and discussed. Improvement due to the introduction of viscoelasticity is evaluated from the comparison to results obtained with the previous elastic method.

2. Experimental

2.1 Material

The investigated material was a short glass fibre reinforced Polyamide 66 with a fibre content of 30% by weight (PA66GF30), provided by Radici Plastics (Italy) as 3.3mm-thick injected plates. Glass fibres had a nominal diameter of 10µm and an average length of 275µm [21]. Their elastic behaviour was ruled by a Young's modulus equal to 72000 MPa and a Poisson ratio equal to 0.22 [6].

The PA66 matrix was a semi-crystalline thermoplastic with viscous mechanical properties, assumed to be viscoelastic in the present work. Details about modelling will be given in section 3.2. PA66 was known to be hydrophilic, with a related sensitivity of physical and mechanical properties to the relative humidity. In order to ensure repeatable state of samples before testing, they were conditioned in a dry-as-moulded state (DAM) in a hermetic chamber. The evolution of the weight of different specimens was measured and only a slight evolution was observed (weight gain of less than 0.3%). Anyway, the weight gain was stabilised before testing.

Injected plates exhibited a classical skin-core microstructure, with a core layer about 400µm-thick and two symmetrical 1.4mm-thick skin layers within which fibres were respectively mainly oriented perpendicularly and parallel to the injection direction. The dogbone specimens (see Fig. 1 for the dimensions**)** used for fatigue tests were cut out from the injected plates with 3 different angles θ to the injection direction: 0, 45 and 90°. Only one specimen was cut per plate in order to ensure the repeatability of the microstructure for the specimens oriented in the same direction. The position of each sample (illustrated in Fig. 1) was such that the central zone was far enough from the injection gate and from the plate sides.

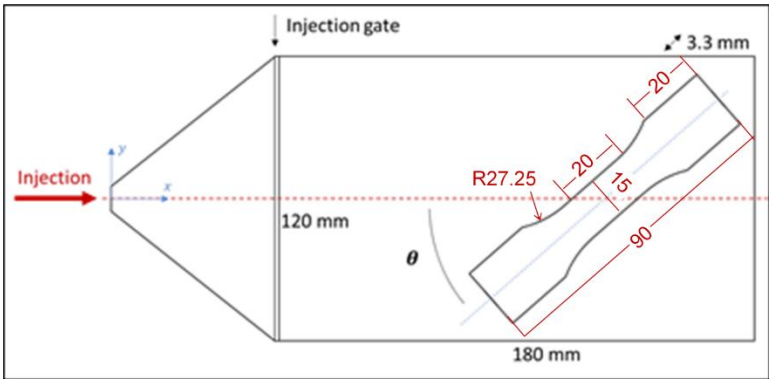

Fig. 1: Location, orientation and dimensions of the specimen cut out from each injected plate for fatigue tests.

2.2 Fatigue testing

Force-controlled fatigue tests were conducted in an INSTRON 8802 hydraulic fatigue machine, equipped with a climatic chamber. Temperature was regulated at 110°C ± 1°C. Prior to fatigue testing, the sample was taken out of the hermetic chamber inside which it was stored in a dry-as-moulded state (DAM) after injection-moulding. It was clamped and fitted with the extensometer. Then the temperature was raised from the ambient up to 110°C for 30 minutes and maintained at 110°C during 45 minutes more, in order to stabilise both the sample temperature and the thermal expansion of the device. The sample was thus considered to be still in a DAM state during testing. The sample was force-controlled at 1MPa during the temperature ramp and plateau.

Fatigue tests were conducted with a sinusoidal signal at constant frequency (2Hz to avoid self-heating) and stress amplitude. Two load ratios (defined as the ratio between the maximum applied stress and the minimum one) were considered: R = 0.1 and R = - 1. A guiding device was used in the latter case, in order to avoid buckling of the dogbone sample [6]. Samples were fitted with an extensometer to measure the macroscopic strain in the loading direction. This was done for both tension and compression loadings. Samples tested at R = 0,1 were fitted with an INSTRON 2620-601 extensometer (12.5mm ±5 mm) on the front face (width of the sample). Due to the presence of the anti-buckling guiding device, samples tested at R = -1 were fitted with an INSTRON 2620-603 extensometer (10 mm ±1 mm) on their side surface (thickness of the sample).

2.3. Results

Fatigue tests were carried out with a double objective. On one hand, fatigue curves constituted the experimental database further used to identify the different parameters of the model and to validate the fatigue life estimation methodology. On the other hand, an analysis of the cyclic

response was conducted to define the input stabilised cycle for the fatigue criterion and identify the constitutive law of the matrix.

a) Fatigue curves

Results in terms of amplitude loading Σ_a as a function of number of cycles to failure, N, are presented as S-N lines in Fig. 2, for the three orientations of samples and the two tested load ratios. The power interpolation lines were described by Basquin's law expressed in equation (1):

$$\Sigma_a = aN^{-b} \quad (1)$$

Only one test was conducted for each level of amplitude stress. However, the very good alignment of the points along the Basquin's lines suggested the low scatter usually observed in SFRT at room ([6], [10], [11], [16], [17]) but also at elevated temperature ([7], [10], [16], [17]).

For both R = 0.1 and R = -1, the resistance to fatigue classically increased with decreasing orientation angles. It resulted from the major alignment of fibres in the loading direction in the thick skin layer. As a proof of the mean stress effect, the resistance was lower for specimens tested at R = 0.1 than for specimens tested at R = -1. This was consistent with the literature either at room temperature ([6], [10], [16]) or at elevated temperature ([7], [16]).

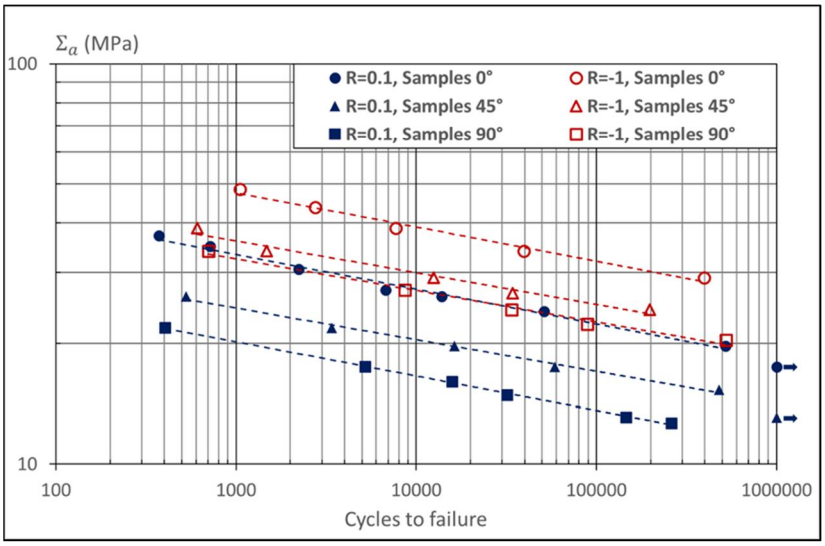

Fig. 2: S-N lines from uniaxial fatigue tests conducted at 110°C for three sample orientations (0, 45 and 90°) and two load ratios (R = 0.1 and R = -1).

b) Cyclic behaviour

In order to apply a fatigue criterion, the input mechanical quantity should be considered as stabilized at least, stationary. It was defined here by considering different parameters measured on the experimental stress Σ -strain e loops whose evolution was followed during the tests. These parameters were the hysteresis area, the secant modulus and the mean strain as defined in Fig. 3 for cycle k.

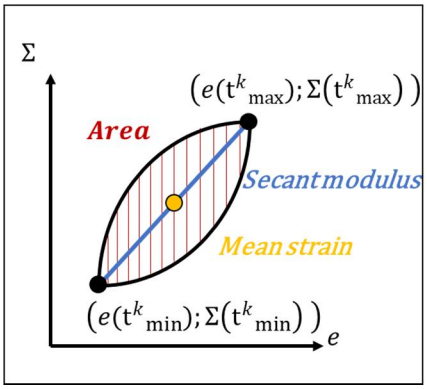

Fig. 3: Schematic representation of the stress-strain loop at cycle k and definition of the parameters associated with stabilization analysis: hysteresis area, secant modulus and mean strain.

The evolution of these parameters was tracked along fatigue tests. Only the evolution of the hysteresis area (linked to the FIP defined later) is represented in Fig. 4, for the three sample orientations (0, 45, and 90°) and the two tested load ratios (R = 0.1 and R = -1).

Curves globally displayed two or three main stages respectively, for tests at R=-1 and R=0.1. In the latter case, an initial transitory step was observed over the very first cycles. It could be explained both by the stabilisation of the force delivered by the hydraulic control and the fact that the stress-strain loops were not closed yet during the first cycles of testing (meaning that the first and last points of the cycle did not coincide). The second stage corresponded to the stabilisation of the hysteresis area and of the secant modulus (not represented here), especially for the tests leading to the longest fatigue lives. Such a stationary state was also observed for short fibre reinforced PA66 at ambient temperature by Jégou et al. [22] and Leveuf et al. [9]. The last stage corresponded to an important loss of stiffness and an important raise of the hysteresis area and the mean strain. This last step could be associated with the propagation of damage leading to the complete failure of the material.

From these observations, the 100th cycle of each curve was considered as representative of the stationary stage. This was particularly true for the longest fatigue lives for which the stabilisation was clearer. Indeed, at the 100th cycle, the evolution rates of the loops parameters between two consecutive cycles did not exceed 0.3% except for two isolated curves corresponding to very low fatigue lives. Moreover, except the softening observed during the four first cycles, the parameters did slightly evolve at the 100th cycle and significantly evolved only in the last percent of the fatigue life (except for very low fatigue lives). This is consistent with a criterion-based design methodology for fatigue lives governed by initiation stage.

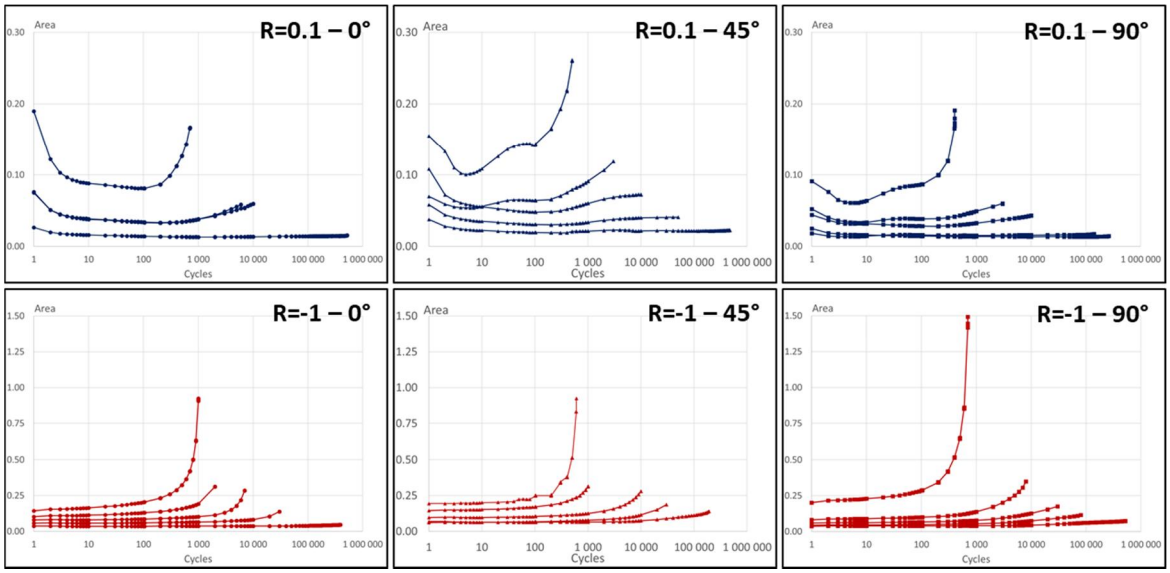

Fig. 4: Evolution of the hysteresis area during the fatigue life at 110°C for each tested sample

3. Fatigue life assessment from TPM methodology

This section aims at presenting successive stages of the TPM with special focus on issues related to its extension to the viscoelastic framework.

3.1 Injection-moulding simulation

Injection-moulding was simulated with Moldflow® software. The output for the following stages of the TPM was a second-order orientation tensor at each integration point of the part.

The simulation giving this second-order orientation tensor needed two family of parameters. The first one was the injection parameters that were given by the material manufacturer. The second one was associated to equations related to the modelling of the fibres motion in a Newtonian flow taking into account the fibres-fibres interaction.

The models available in Moldflow® were the model of Folgar-Tucker [23] and the Reduced Strain Closure (RSC) model [24] (based on [25]). The associated equations were dependent on

the fourth-order orientation tensor constructed from the second-order one with an hybrid closure approximation [26], [27]. The model used in the present work was the RSC model and needed two parameters, C_I and κ. The parameter C_I is called the interaction coefficient while $1/\kappa$ is the strain reduction factor. Their identification was done by comparing measurements of the principal components of the second-order orientation tensor and corresponding numerical predictions on different zones of the injected plates. Experimental observations were done by P. Hine (Leeds University, UK) following a methodology described in [28]. Special attention was paid to ensure the best agreement as possible between experimental values and predictions in the region from which samples were cut out (Fig.1). In this area, fibres were homogeneously oriented both in the skin and core layers, respectively in the injection direction and perpendicularly to it. In the first third of the plate, close to the gate, they were homogeneously oriented too in the skin layers but not in the core one. The values finally obtained were: $C_I = 0.009$, $\kappa = 0.41$.

3.2 Local mechanical properties estimates as a function of fibre orientation distribution

a) Orientation transfer - Viscoelastic homogenization

The second stage of the TPM was the estimate of the homogenized viscoelastic properties at each point of the model used for FE analysis. Prior to this stage, the orientation tensor components had to be transferred from the Moldflow® model to the FE (Abaqus®) model. Digimat®-MAP software was used to this aim. The receiver mesh (Abaqus®) was generated with the same type of elements and average mesh size (1mm) as the donor mesh (Moldflow®). In order to optimize the quality of the transfer, special attention was paid to the region from which the samples were cut out. The aim was to have a regular mesh and identical to the donor one.

The viscoelastic homogenisation was processed with Digimat®-MF [29] according to a classical procedure. The linear viscoelastic heterogeneous problem was turned into a symbolic linear elastic problem by using the Laplace-Carson transform. This elastic problem was solved in the Laplace domain by a linear scheme before coming back to the real time domain using the collocation method. The linear homogenization model was based on the Mori-Tanaka scheme and on an orthotropic closure approximation to compute the fourth-order orientation tensor from the second-order one provided by the injection simulation. This procedure was linked to the viscoelastic FE simulation at each time step as explained in section 3.3.

The input data for viscoelastic homogenization were the properties of each phase (elastic glass fibres and viscoelastic PA66) and the morphological characteristics of the composite (i.e. the aspect ratio, volume ratio and local second-order orientation tensor of fibres at any point). They are detailed in the next sub-section.

b) Constituents properties

The properties for the glass fibres (Young's modulus E = 72000 MPa ; Poisson ratio $\nu = 0.22$) were supposed identical at room temperature and at 110°C. They were issued from [6]. The aspect ratio, calculated from the average length and diameter given in the work of Bernasconi et al. [11], was equal to 0.275. The volume ratio of fibres was deduced from the mass ratio, the density of glass (2540 kg/m3 [30]) and the density of PA66 (1360 kg/m^3 [5]).

The matrix was considered as linear viscoelastic and isotropic following the Prony series representation available in Digimat®. The shear and bulk relaxation moduli $G(\mathrm{t})$ and $K(\mathrm{t})$ were thus defined in the following way:

$$G(t) = G_0\left[1 - \sum_{i=1}^{n} g_i\left(1 - e^{-t/\tau_i}\right)\right], \qquad g_i = \frac{G_i}{G_0} \tag{2}$$

$$K(t) = K_0\left[1 - \sum_{i=1}^{n} k_i\left(1 - e^{-t/\tau_i^*}\right)\right], \qquad k_i = \frac{K_i}{K_0} \tag{3}$$

with G_0, K_0 the initial glassy moduli, g_i and k_i the shear and bulk weight factors, and G_i and K_i the shear and bulk moduli associated to relaxation times τ_i and τ_i^*, respectively. The number of relaxation times was not limited but in order to reduce calculation time, it had to be low.

It was well known that the behaviour of the thermoplastic polymer within the composite differed from that of the bulk polymer. Consequently, the identification of the matrix viscoelastic law relied on macroscopic data obtained from the testing of composite samples. This identification strategy was also designed in accordance with the choices made for further stages of the TPM. The FIP involved in the employed fatigue criterion (fourth stage of the TPM, section 3.4) was the dissipated energy over one cycle that should be representative of a stabilized, at least stationary, state. It has been observed (section 2.3-b) that the 100th cycle could be considered as representative of a stationary cycle. However, and following the idea of Klimkeit et al. as a first attempt, the FIP was deliberately computed over the first closed cycle, corresponding to the second one. This choice was motivated by the industrial application context, requiring a minimum number of cycles to be simulated, and the expected inability of the viscoelastic framework to reproduce the composite cyclic behaviour until stabilisation. To give more sense to this strong simplification, the matrix viscoelastic law was identified in such a way that the 2nd macroscopic simulated cycle coincides with the 100th experimental one. In some manner, this strategy led to the building of an "equivalent" composite whose second cycle was aimed to approach the 100th ("stabilized") cycle of the real composite. In such a strategy, it seemed reasonable to consider only three relaxation times for the matrix law which offered also the advantage to minimize the computational time.

Due to the lack of multiaxial tests, the difference between Prony parameters associated to shear and bulk moduli could not be documented. Thus, the relaxation times and weights were supposed to be the same for the bulk and shear moduli. Relaxation times were set within 2 decades centred on the duration of 1 loading cycle (0.5s at 2Hz). Initial values for the instantaneous and relaxed moduli were deduced from the 100th experimental cycle of the samples undergoing the highest and lowest strain rates. Then, the identification process was based on the samples exhibiting the two longest fatigue lives for each of the three orientations and each load ratio. More precisely, the identification was conducted by minimizing the relative error on macroscopic hysteresis area and secant modulus between the 100th experimental cycle and the 2nd simulated one for these twelve samples. The simulation was done using Digimat®-Abaqus® and the axial strain was deduced from the relative displacement of 2 nodes located as close as possible to the position of the two knives of the experimental extensometer. The macroscopic axial stress was calculated from the applied force divided by the initial cross-section area of the sample as for experiments.

Table 1 presents the parameters finally obtained.

	$G_0 = 226.5\ MPa$	$K_0 = 11250\ MPa$
$\tau_i = \tau_i^*$	g_i	k_i
0.05	0.156	0.156
0.5	0.0496	0.0496
5	0.0169	0.0169

Table 1: Parameters of the Prony series for the matrix viscoelastic law.

The relative error (defined as the difference between the numerical and the experimental values divided by the experimental one) fluctuated between 7 and 36% for the hysteresis area, and between 1 and 26% for the secant modulus. As an illustration of the quality of the identification, Fig 5 compares the 2nd macroscopic simulated cycle to the 100th experimental one in the best of the twelve situations regarding the relative error on the hysteresis area (7% at R = -1 and 90°

in Fig. 5(a)) and the worst one (36% at R = -1 and 0° in Fig. 5(b)). As only 2 loading cycles were simulated, the mean strain evolution could not be considered directly. In these graphs, the mean strain was artificially shifted to make the comparison easier.

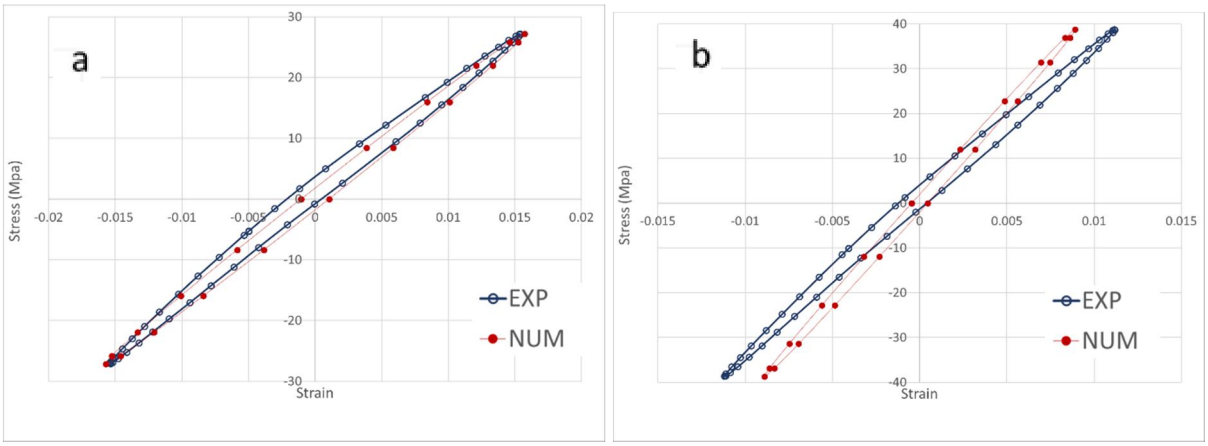

Fig. 5: Comparison between the 2nd macroscopic simulated cycle and the 100th experimental cycle. a: sample oriented at 90° - R = -1. b: sample oriented at 0° - R = -1.

3.3 Finite Element Analysis

The FE analysis was performed with Abaqus® using a Digimat® plugin giving the local homogenised mechanical properties at each time step of loading. The sample was meshed with 2D triangular shell elements S3, divided into 20 layers through the thickness of the sample, with three integration points (IP) in each layer. For each layer of each element, the corresponding fibre orientation tensor was attached. This means that the same orientation tensor was attached to the three IP of each layer of an element. In the sample plane, the mesh size was set at 1mm, for matching purpose with the injection-moulding simulation with Moldflow® and thus minimize the interpolation error during the transfer of the orientation tensor. For the same reason, the triangular shape of the elements matched the Moldflow® model.

The FE simulations were conducted with the same loading profile (sinusoidal wave form, frequency, maximal applied load, load ratio,…) and boundary conditions as the experiments. As explained above, only two cycles were simulated. The load was applied to a single node of the lower head of the sample, tied to all the nodes in the head; only translation in the direction of loading was allowed. The upper head was clamped and thus fully constrained (6 degrees of freedom were locked).

3.4 Fatigue criterion

a) Formulation and FIP calculation

Assuming that the dissipated energy was the mechanical quantity monitoring the fatigue life, the criterion of Jegou et al. [22] was selected. It was written as follows:

$$\Delta^* = CN^{-b} \tag{4}$$

with Δ^* the dissipated energy over one cycle (that should be stabilized), N the number of cycles to failure and b and C two material parameters. As previously done by Klimkeit et al. [6] for the elastic energy-based criterion, a specific parameter f was added to take into account the mean stress effect. This parameter was calculated from the solving of an empirical equation proposed by Kujawski and Ellyin [31]:

$$f^2 - \frac{\sigma_m}{\sigma_a} f - 1 = 0 \tag{5}$$

where σ_m and σ_a are respectively the mean and amplitude stresses characterizing the macroscopic fatigue loading. The positive solution of the previous equation was taken and the fatigue criterion became:

$$f\Delta^* = CN^{-b} \quad (6)$$

The input mechanical quantity (FIP) for the fatigue criterion was thus $f\Delta^*$. f was given by solving equation (5) and only depended on the macroscopic load ratio while Δ^* had to be evaluated from the post-processing of the FE analysis. The dissipated energy per unit volume over one cycle was here assimilated to the mechanical energy received over the cycle (nullity of the stored energy). In the particular case of a uniaxial stress state, this would have consisted in assimilating the dissipated energy over the cycle to the hysteresis area of the axial stress-strain response as commonly done in the literature. It must be reminded that local stress state within a sample, even under uniaxial macroscopic loading, is potentially multiaxial due to the local fibre orientation distribution and specimen geometry. This is even truer for injected parts with complex geometry.

In this paper, as a first approach devoted to uncouple the different effects, the application method of the fatigue criterion, for both its identification and further validation of the whole TPM, followed the same principle as the one proposed by Klimkeit et al. [6]. The local dissipated energy over the second simulated cycle, assimilated to the received mechanical energy, was indeed averaged over the volume of each element of the specimen. Then, Δ^*, used as input for the criterion, was the maximum value obtained over all the elements of the model:

$$\Delta^* = \underset{elements}{\mathrm{Max}} \langle D \rangle_{V_e} \quad \text{with} \quad D = \oint_{2\text{nd cycle}} \bar{\bar{\sigma}} : \dot{\bar{\bar{\epsilon}}}\, dt \quad (7)$$

A Python scrypt has been specifically developed in order to compute (i) the received energy over the second cycle at each integration point, then (ii) the average over the volume of each element and (iii) finally the search of the maximum value within the part and corresponding element.

b) Identification of the criterion parameters

The fatigue criterion (equation (6)) required one S-N line for the identification of both material parameters C and b. Following the previous work in elasticity [6], the S-N line of the specimens oriented at 0° and loaded at R = -1 was chosen. The mean stress correction via f was thus inactive ($f = 1$ according to equation (5)).

The TPM was applied to the selected specimen (0° orientation) for all the stress levels of the experimental S-N line. Then, the FIP, Δ^*, calculated according to the foregoing methodology (section 3.4-a), was plotted against the experimental number of cycles to failure (in log-log scale). The interpolation equation directly provided the parameters C and b of the fatigue criterion: $C = 0.346$ and $b = 0.171$. The influence of the S-N line chosen for the identification of the fatigue criterion will be discussed in the next section.

4. Results and discussion

The TPM has been applied to every specimen and loading condition of the whole database available at 110°C. Results are presented in the following with two angles, the prediction of the locations of fatigue failure and the prediction of the fatigue lives.

4.1 Failure initiation location

The post-process of mechanical fields, as described in section 3.4-a, allowed to get the average received mechanical energy in each element of a loaded specimen and to identify the element exhibiting the maximal value. Fig. 6 and Fig. 7 display maps of the average energy for R = 0.1 and R = -1 respectively, at stress levels leading to the longest lifetime for each of the three fibre

orientations. Maxima are marked with blue dots.

In all cases, “hot points” were located in the fillets of the specimens. For the specimens oriented at 0° and 90°, the 4 filets were hot points. However, gradients were stronger for the 0° sample than for the 90° one. In the latter case, the fatigue indicator was more homogeneous within the gauge length. Due to the fibre orientation in specimens at 45°, only the top right and bottom left fillets were hot points. The combined effects of fibre orientation and geometry of the specimen led to higher stress concentration at these points. The effect of the load ratio was mainly related to the values of energy reached: at R = 0.1, maximal stresses were higher than those obtained at R = -1.

Fig. 8 displays views of samples broken after testing at R = 0.1 and R = -1 and exhibiting the longest fatigue lives for each orientation. Most of the specimens failed in the fillets (top or bottom) except samples oriented at 90° and tested at R = 0.1 that failed in the middle. It could be related to the weaker heterogeneity of the average energy in these samples, as evidenced from the FE simulation in Fig.6. Indeed, when gradients are weaker, other potential sources of experimental variability may better express and lead to the failure.

The comparison between experiment and simulation showed that this energy could be a good driving parameter to predict the location of the less resistant areas to fatigue loading.

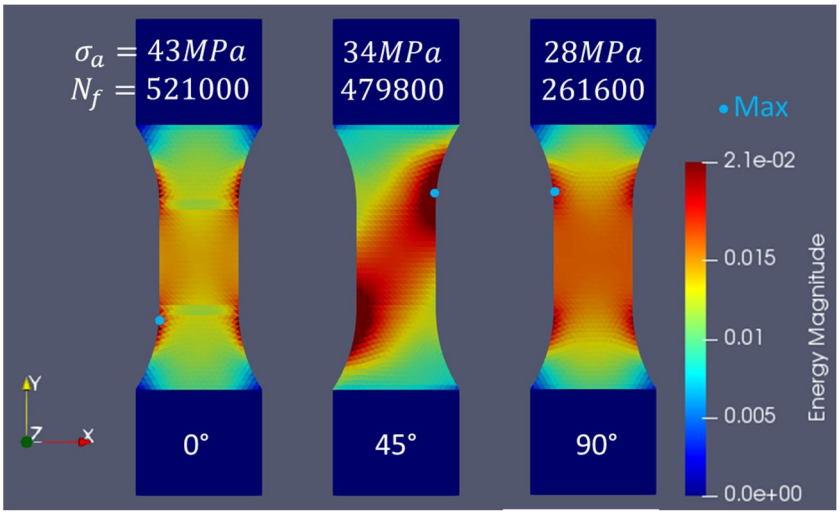

Fig. 6: Mapping of the simulated energy (averaged over the volume of each element) for three specimens (0, 45 and 90°) tested at R = 0.1 and exhibiting the longest fatigue life. The element displaying the maximum of average energy (mJ/mm^3) is marked with blue dot.

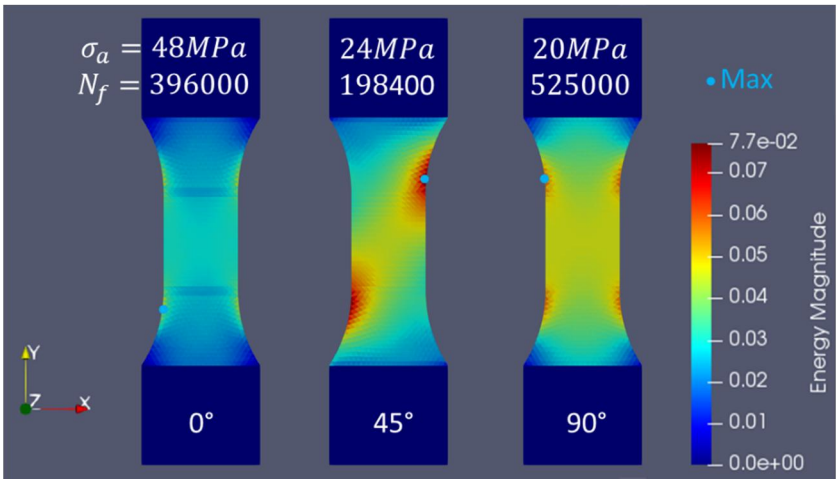

Fig. 7: Mapping of the simulated energy (averaged over the volume of each element) for three specimens (0, 45 and 90°) tested at R = -1 and exhibiting the longest fatigue life. The element displaying the maximum of average energy (mJ/mm^3) is marked with blue dot.

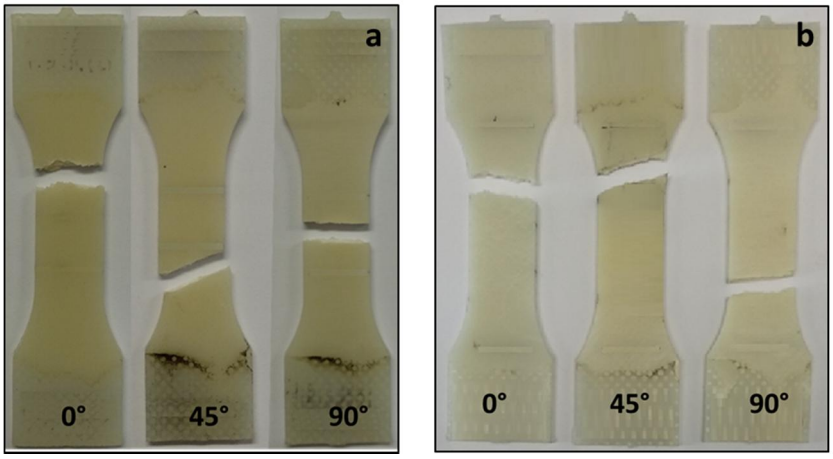

Fig. 8: Failure locations of samples tested at (a) R = 0.1 and (b) R = -1 and exhibiting the longest fatigue life.

4.2 Comparison of experimental and simulated fatigue lives

For each sample and loading condition, the knowledge of the maximal value Δ^* of the average energy over all the elements of the sample allowed estimating the simulated number of cycles to failure $N_{calculated}$ as follows:

$$N_{calculated} = \exp\left(\frac{\ln(C) - \ln(f\Delta^*)}{b}\right) \quad (8)$$

where f was deduced by solving equation (5) for the load ratio considered and, b and C were identified by applying the TPM to the samples with 0° orientation, tested at R=-1 and using the corresponding S-N line (see section 3.4-b). The number of cycles $N_{calculated}$ was compared to the number of cycles to failure experimentally obtained ($N_{experimental}$). Results are shown in Fig 9. The perfect prediction is the line driven by the equation $N_{calculated} = N_{experimental}$. This line is the limit between conservative results ($N_{calculated} < N_{experimental}$) and non-conservative results ($N_{calculated} > N_{experimental}$). The thin dashed lines represent a difference of + or – 1 decade with the perfect prediction line while the thick dashed lines correspond to a

difference of + or – 2 decades.

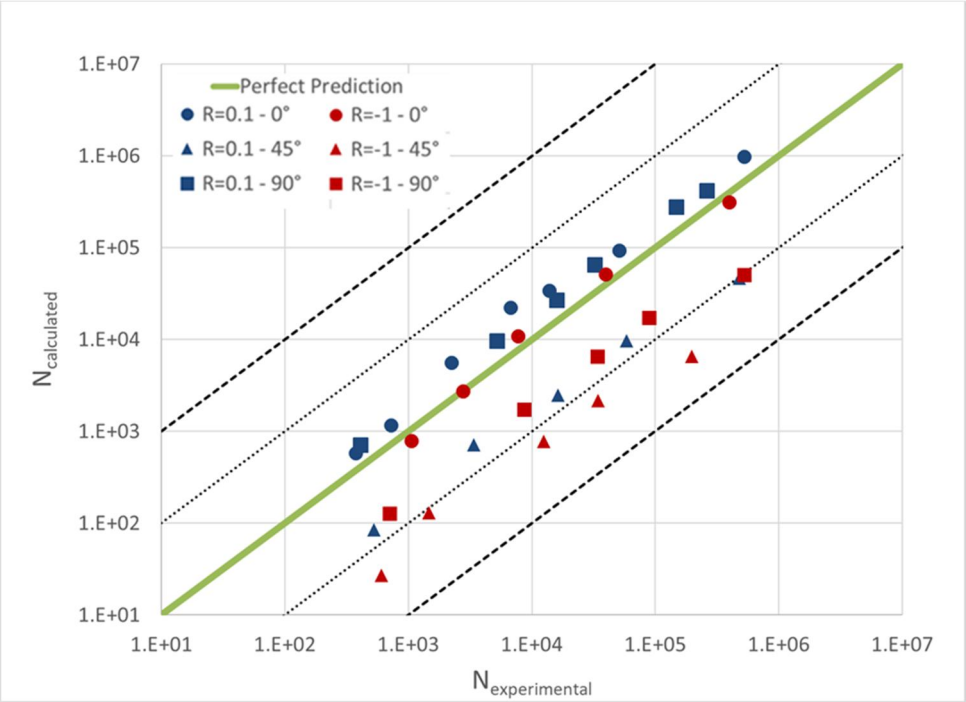

Fig. 9: Results of the fatigue life assessment methodology (TPM) at 110° C in the viscoelastic framework: simulated against experimental numbers of cycles to failure.

For each orientation and load ratio, results were either conservative (in the limit of 1 decade except for the samples oriented at 45° and tested at $R = -1$) or very close to the perfect prediction (in the limit of +1 decade for the samples oriented at 0° and 90° and tested at $R = 0.1$).

In order to quantify the benefit of the viscoelastic framework compared to the elastic one, the TPM in its elastic version due to Klimkeit et al. [6] has been applied to the whole database at 110°C. The same fibre orientation distribution was used for FE analysis. Elastic properties at 110°C of the PA66 matrix, issued from the supplier, were: E = 530MPa, ν = 0.49, while the properties of the fibres were unchanged. The Mori-Takana scheme and the same closure approximation as in section 3.2-a were employed for the elastic homogenization. At last, the fatigue criterion, (equation (6)) with the elastic energy replacing the dissipated energy, was

applied with the same averaging process (volume average of the energy over each element and search for the maximum value). Using the same S-N line and procedure as in section 3.4-b, the parameters of the elastic energy-based fatigue criterion were obtained: C = 1.532 and b = 0.171. Simulated fatigue lives finally obtained with the elastic TPM are plotted as functions of the experimental values in Fig. 10. Prediction were particularly poor at R = 0.1 with a difference to the perfect prediction larger than 3 decades (against 1 with the extended, viscoelastic, TPM). More generally, results obtained for the 3 orientations and 2 load ratios were better unified in the viscoelastic framework (Fig. 9) than in the elastic one (Fig. 10).

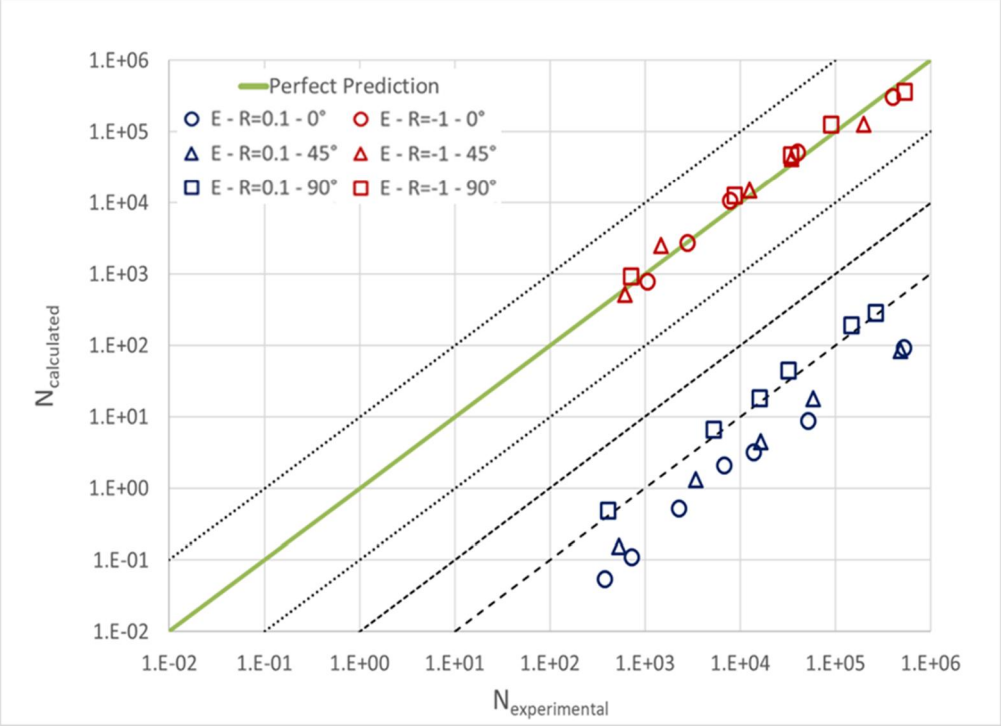

Fig. 10 : Results of the fatigue life assessment methodology (TPM) at 110° C in the elastic framework: simulated against experimental numbers of cycles to failure.

In the following, a discussion is proposed regarding two issues. The first one is related to the fatigue criterion (mean stress correction and parameters identification) and the second one regards the matrix viscoelastic law.

Regarding the first point, Fig. 11 shows the predictions obtained with the viscoelastic TPM by applying the fatigue criterion without mean stress correction, equation (4). It must be noted that the criterion parameters, previously identified in section 3.4-b on specimens oriented at 0° and loaded at R = -1, were unchanged. The comparison between Fig. 11 and Fig. 9 clearly illustrates the improvement provided by the empirical mean stress correction due to [31], as previously observed in elasticity by Klimkeit et al. [6]. Predictions obtained at R= 0.1 with mean stress correction (Fig. 9) are much better and the difference between the results obtained for both load ratios is reduced. However, some work is still necessary to enhance the description of the mean stress effect.

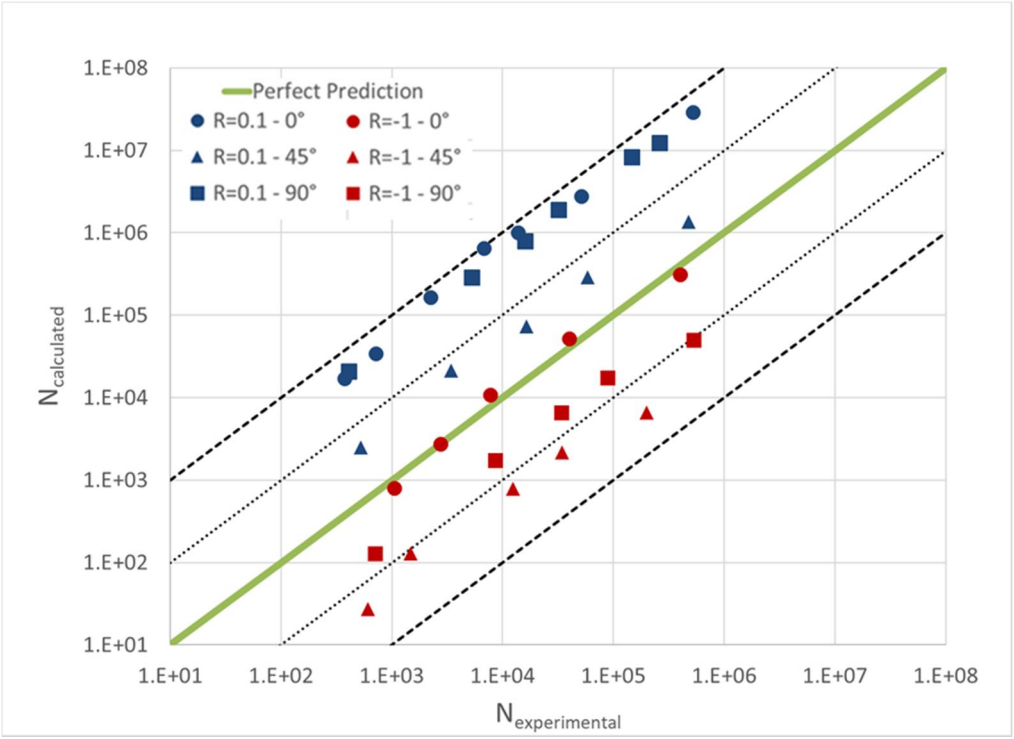

Fig. 11: Results of the fatigue life assessment methodology (TPM) at 110°C in the viscoelastic framework without mean stress correction: simulated against experimental number of cycles to failure.

In order to appreciate the influence of the S-N line chosen for the criterion identification, Fig. 12 plots the simulated FIP, $f\Delta^*$, against the experimental number of cycles to failure for all the loading conditions and specimen orientations. The lines are the power interpolations for each

specimen orientation and load ratio, from which the criterion parameters b and C could be identified. In the foregoing (section 3.4-b), the line corresponding to the specimens with 0° orientation loaded at R = -1 was chosen for the criterion identification. As shown in Fig. 12, every curve displayed the same slope (parameter b), only the level of energy differs (parameter C). Since the slope is the same, choosing one curve or another to identify the criterion parameters would only lead to a translation of the predicted fatigue lives. The scatter as well as the orientation and mean stress effects would stay the same than in Fig. 9. The choice of the specimens oriented at 0° for a load ratio of R = -1 led to get most of the results within a limit of 1 decade from the perfect prediction. Even if some predictions were slightly non-conservative, this choice appeared as relevant. An identification from the experimental S-N line 0°/R = 0.1 would translate the points down in Fig. 9. All the results would be conservative but with a strong underestimation of the fatigue lives of the specimens 45° - 90°/R = -1.

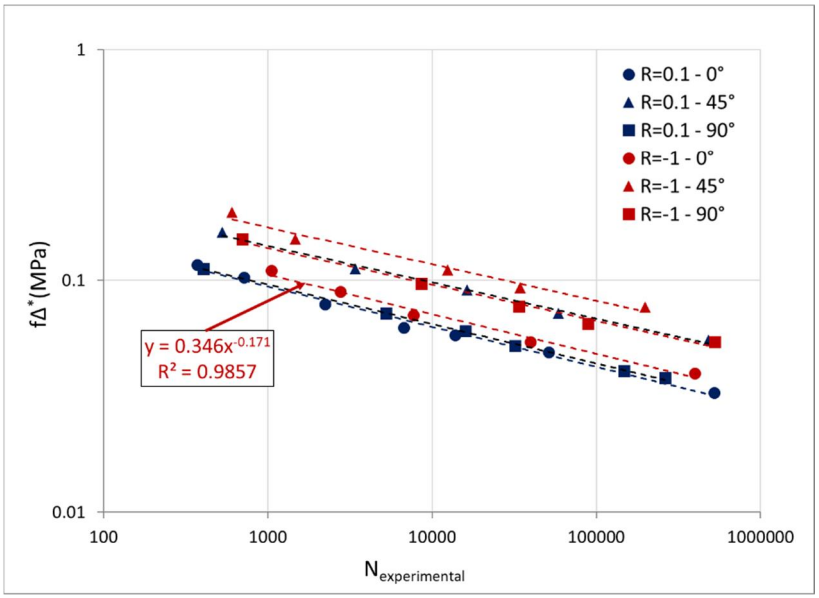

Fig. 12: Simulated FIP as a function of the experimental number of cycles to failure.

At last, improvement of the present methodology could arise from a better identification of the constitutive law of the matrix. As a first step, the numerical identification itself could be optimized.

More generally, in accordance with fundamental knowledge of polymer viscoelasticity, relaxation times should be differentiated for the bulk and shear generalized moduli in the Prony series. To this aim, fatigue tests along other loading paths, like shear tests, should be included to the database.

Nevertheless, since the matrix viscoelastic law was extracted from a micromechanical analysis of the composite behaviour, it was never identified from pure uniaxial loading, even from a basic macroscopic tensile test. Identification from tensile tests already resulted from a compromise between various local states in the matrix, due to the local disorientation of fibres. But, by integrating shear or fatigue tests to the database for the constitutive law of the matrix, a broader set of multiaxial states would be accessible and make possible a separate identification of bulk and shear relaxation times. At last, some fatigue data involving negative load ratios should also be added.

5. Conclusion

The main goal of this study was to integrate the viscoelastic behaviour of the PA66 matrix in a through-process modelling method for fatigue life estimation of Short Fibre Reinforced Thermoplastics at high temperature. In order to keep a rather easy-to-use method for industrial components, the method was based on a chain of commercial softwares (MoldFlow®, Digimat® and Abaqus®).

The fatigue test database was obtained from tensile tests in PA66GF30 dogbone specimens machined out from injection-moulded plates, with three different orientations to the injection direction: 0, 45 and 90°. Force-controlled fatigue test were performed at 110°C in Dry-As-Moulded specimens, under constant amplitude and frequency (2Hz) and two load ratios (0.1 and -1).

At any point of the sample, the anisotropic viscoelastic response was estimated (Abaqus® software coupled to a Digimat® plug-in) from a micromechanical calculation based on the morphology of the composite, the fibres elastic behaviour and the matrix viscoelastic one. The orientation tensor of fibres was transferred from MoldFlow® simulation of injection-moulding. A systematic analysis

of the stabilization of the macroscopic experimental stress-strain loop showed that a stationary state was reached after 100 cycles for all tests in the database. Therefore, the PA66 matrix viscoelastic law (expressed via Prony series on the bulk and shear moduli) was identified so that the second macroscopic simulated cycle corresponded to the stabilized one. The number of relaxation times could then be reduced to three. The Fatigue Indicator Parameter (FIP), chosen as the dissipated energy (assimilated to the received energy) over the stabilized cycle, was computed at any integration point using the local three-dimensional strain and stress tensors over this cycle, and averaged over the thickness of each element. The resulting maximum value of the FIP over all the elements was the input quantity of the fatigue criterion, expressed as a power law of the number-of-cycles-to-failure.

Maps of the FIP showed that the critical zones were located in the fillets of the specimen, as observed experimentally. The predicted number-of-cycles-to-failure were compared to the experimental ones. Results were close within one decade to the perfect prediction. It was shown that the introduction of viscoelasticity significantly improved the quality of predictions, compared to results obtained from the similar approach in a purely elastic framework. This is a noticeable result that could be improved now from a better calibration of the matrix constitutive law. The fatigue criterion itself should be reconsidered also to better capture mean stress effect. The mean stress correction model proposed by Eftekhari and Fatemi [32] could be used to this aim. Investigation on the application method of the criterion is under progress in the case of macroscopic singularities like notches or ribs.

Acknowledgements

Direction Générale de l'Armement (convention DGA n°3014.60.0058) and Région Poitou-Charentes are gratefully acknowledged for the PhD grant of Nathan Fouchier. Dr Irène Maillet and Dr Matthieu Guehenec from DGA are gratefully acknowledged for fruitful discussions.

Computations have been performed on the supercomputer facilities of the Mesocentre de calcul SPIN Poitou- Charentes. Experiments were partly supported by funding from the European Community (FEDER FSE project HYGROPOLYM ref P-2017-BAFE-117).

References

[1] N. Despringre, Y. Chemisky, K. Bonnay, and F. Meraghni, 'Micromechanical modeling of damage and load transfer in particulate composites with partially debonded interface', *Composite Structures*, vol. 155, no. Supplement C, pp. 77–88, Nov. 2016.

[2] A. Krairi, I. Doghri, and G. Robert, 'Multiscale high cycle fatigue models for neat and short fiber reinforced thermoplastic polymers', *International Journal of Fatigue*, vol. 92, no. Part 1, pp. 179–192, Nov. 2016.

[3] H. Nouri, F. Meraghni, and P. Lory, 'Fatigue damage model for injection-molded short glass fibre reinforced thermoplastics', *International Journal of Fatigue*, vol. 31, no. 5, pp. 934–942, May 2009.

[4] S. Kammoun, I. Doghri, L. Brassart, and L. Delannay, 'Micromechanical modeling of the progressive failure in short glass–fiber reinforced thermoplastics – First Pseudo-Grain Damage model', *Composites Part A: Applied Science and Manufacturing*, vol. 73, no. Supplement C, pp. 166–175, Jun. 2015.

[5] A. Launay, M. H. Maitournam, Y. Marco, and I. Raoult, 'Multiaxial fatigue models for short glass fibre reinforced polyamide. Part II: Fatigue life estimation', *International Journal of Fatigue*, vol. 47, no. Supplement C, pp. 390–406, Feb. 2013.

[6] B. Klimkeit *et al.*, 'Multiaxial fatigue life assessment for reinforced polymers', *International Journal of Fatigue*, vol. 33, no. 6, pp. 766–780, Jun. 2011.

[7] C. M. Sonsino and E. Moosbrugger, 'Fatigue design of highly loaded short-glass-fibre

reinforced polyamide parts in engine compartments', *International Journal of Fatigue*, vol. 30, no. 7, pp. 1279–1288, Jul. 2008.

[8] A. Wilmes and K. Hornberger, 'Influence of Fiber Orientation and Multiaxiality on the Fatigue Strength of Unnotched Specimens – Lifetime Estimation', *Procedia Engineering*, vol. 133, pp. 148–160, Jan. 2015.

[9] L. Leveuf, Y. Marco, V. Le Saux, L. Navrátil, S. Leclercq, and J. Olhagaray, 'Fast screening of the fatigue properties of thermoplastics reinforced with short carbon fibers based on thermal measurements', *Polymer Testing*, vol. 68, pp. 19–26, Jul. 2018.

[10] S. Mortazavian and A. Fatemi, 'Fatigue behavior and modeling of short fiber reinforced polymer composites including anisotropy and temperature effects', *International Journal of Fatigue*, vol. 77, no. Supplement C, pp. 12–27, Aug. 2015.

[11] A. Bernasconi, P. Davoli, A. Basile, and A. Filippi, 'Effect of fibre orientation on the fatigue behaviour of a short glass fibre reinforced polyamide-6', *International Journal of Fatigue*, vol. 29, no. 2, pp. 199–208, Feb. 2007.

[12] Y. Zhou and P. K. Mallick, 'Fatigue Performance of an Injection-Molded Short E-Glass Fiber-Reinforced Polyamide 6,6. I. Effects of Orientation, Holes, and Weld Line', 2006.

[13] M. De Monte, E. Moosbrugger, K. Jaschek, and M. Quaresimin, 'Multiaxial fatigue of a short glass fibre reinforced polyamide 6.6 – Fatigue and fracture behaviour', *International Journal of Fatigue*, vol. 32, no. 1, pp. 17–28, Jan. 2010.

[14] K. Noda, A. Takahara, and T. Kajiyama, 'Fatigue failure mechanisms of short glass-fiber reinforced nylon 66 based on nonlinear dynamic viscoelastic measurement', *Polymer*, vol. 42, no. 13, pp. 5803–5811, Jun. 2001.

[15] A. Benaarbia, A. Chrysochoos, and G. Robert, 'Thermomechanical behavior of PA6.6 composites subjected to low cycle fatigue', *Composites Part B: Engineering*, vol. 76, no. Supplement C, pp. 52–64, Jul. 2015.

[16] A. Launay, Y. Marco, M. H. Maitournam, and I. Raoult, ‘Modelling the influence of temperature and relative humidity on the time-dependent mechanical behaviour of a short glass fibre reinforced polyamide’, *Mechanics of Materials*, vol. 56, no. Supplement C, pp. 1–10, Jan. 2013.

[17] S. Barbouchi, ‘Effect of water on the fatigue behaviour of a pa66/glass fibers composite material’, *Journal of Materials Science*, vol. 42, no. 6, pp. 2181–2188, 2007.

[18] A. Launay, M. H. Maitournam, Y. Marco, and I. Raoult, ‘Multiaxial fatigue models for short glass fiber reinforced polyamide – Part I: Nonlinear anisotropic constitutive behavior for cyclic response’, *International Journal of Fatigue*, vol. 47, no. Supplement C, pp. 382–389, Feb. 2013.

[19] Y. Marco *et al.*, ‘Dissipation analysis in SFRP structural samples: Thermomechanical analysis and comparison to numerical simulations’, *International Journal of Fatigue*, vol. 67, no. Supplement C, pp. 142–150, Oct. 2014.

[20] A. Selmi, I. Doghri, and L. Adam, ‘Micromechanical simulations of biaxial yield, hardening and plastic flow in short glass fiber reinforced polyamide’, *International Journal of Mechanical Sciences*, vol. 53, no. 9, pp. 696–706, Sep. 2011.

[21] A. Bernasconi, D. Rossin, and C. Armanni, ‘Analysis of the effect of mechanical recycling upon tensile strength of a short glass fibre reinforced polyamide 6,6’, *Engineering Fracture Mechanics*, vol. 74, no. 4, pp. 627–641, Mar. 2007.

[22] L. Jégou, Y. Marco, V. Le Saux, and S. Calloch, ‘Fast prediction of the Wöhler curve from heat build-up measurements on Short Fiber Reinforced Plastic’, *International Journal of Fatigue*, vol. 47, no. Supplement C, pp. 259–267, Feb. 2013.

[23] F. Folgar and C. L. Tucker, ‘Orientation Behavior of Fibers in Concentrated Suspensions’, *Journal of Reinforced Plastics and Composites*, vol. 3, no. 2, pp. 98–119, Apr. 1984.

[24] J. Wang, J. F. O’Gara, and C. L. Tucker, ‘An objective model for slow orientation kinetics

in concentrated fiber suspensions: Theory and rheological evidence', *Journal of Rheology*, vol. 52, no. 5, pp. 1179–1200, Sep. 2008.

[25] G. B. Jeffery, 'The motion of ellipsoidal particles immersed in a viscous fluid', *Proc. R. Soc. Lond. A*, vol. 102, no. 715, pp. 161–179, Nov. 1922.

[26] Moldflow, 'Moldflow's fiber orientation models (Theory), Moldflow Flex 2016, Autodesk Knowledge Network', 2018. [Online]. Available: https://knowledge.autodesk.com/support/moldflow-flex/learn-explore/caas/CloudHelp/cloudhelp/2016/ENU/MoldflowInsight360/files/GUID-6B3A7386-DE57-450E-BF94-B10BD629EC9B-htm.html. [Accessed: 07-Oct-2018].

[27] S. G. Advani and C. L. Tucker, 'Closure approximations for three-dimensional structure tensors', *Journal of Rheology*, vol. 34, no. 3, pp. 367–386, Apr. 1990.

[28] P. J. Hine, N. Davidson, R. A. Duckett, and I. M. Ward, 'Measuring the fibre orientation and modelling the elastic properties of injection-moulded long-glass-fibre-reinforced nylon', *Composites Science and Technology*, vol. 53, no. 2, pp. 125–131, Jan. 1995.

[29] Digimat, *Digimat - User's Manual - v2016*. 2016.

[30] B. Klimkeit, 'Etude expérimentale et modélisation du comportement en fatigue multiaxiale d'un polymère renforcé pour application automobile', PhD. thesis, ENSMA, 2009.

[31] D. Kujawski and F. Ellyin, 'A unified approach to mean stress effect on fatigue threshold conditions', *International Journal of Fatigue*, vol. 17, no. 2, pp. 101–106, Feb. 1995.

[32] M. Eftekhari and A. Fatemi, 'Fatigue behaviour and modelling of talc-filled and short glass fibre reinforced thermoplastics, including temperature and mean stress effects', *Fatigue & Fracture of Engineering Materials & Structures*, vol. 40, pp.333–348, 2017.